

General Shiba mapping for on-site four-point correlation functions

Herbert Eßl,^{1,*} Matthias Reitner¹,,¹ Giorgio Sangiovanni²,,² and Alessandro Toschi¹

¹*Institute of Solid State Physics, TU Wien, 1040 Vienna, Austria*

²*Institut für Theoretische Physik und Astrophysik and Würzburg-Dresden Cluster of Excellence ct.qmat, Universität Würzburg, 97074 Würzburg, Germany*



(Received 20 March 2024; accepted 17 June 2024; published 15 July 2024)

By applying the Shiba mapping on the two-particle level, we derive the relation between the local four-point correlation functions of bipartite lattice models with on-site electronic repulsion and those of the corresponding models with attractive interaction in the most general setting. In particular, we extend the results of [Phys. Rev. B **101**, 155148 (2020)], which were limited to the rather specific situation of the static limit in strictly particle-hole symmetric models, (i) by explicitly including *both* magnetic field and different values of the chemical potentials, and (ii) by considering the full dependence of the generalized susceptibilities on the transfer (bosonic) Matsubara frequency. The derived formalism is then applied, as a relevant benchmark, to the Hubbard atom by investigating the general properties of the divergences of its irreducible vertex functions as a function of chemical potential and applied magnetic field. The resulting phase diagrams provide an insightful compass for future studies of the breakdown of the self-consistent perturbation expansion beyond high-symmetric regimes.

DOI: [10.1103/PhysRevResearch.6.033061](https://doi.org/10.1103/PhysRevResearch.6.033061)

I. INTRODUCTION

Due to the impressive algorithmic and computational advancements of the past decade, performing quantum-many body calculations of four-point correlation functions has become achievable also in nontrivial, strongly correlated parameter regimes. Evidently, this progress is highly relevant for several reasons. Among these are the precise calculations of vertex corrections of physical susceptibilities [1–5] and conductivities [6–8], the identification of the predominant scattering mechanisms underlying intriguing photoemission or self-energy features [9–14], and the implementation of advanced diagrammatic expansions [15–19] for nonperturbative regimes.

On the theoretical side, this development has triggered a quest for improving our fundamental understanding of the many-electron properties on the two-particle level and their associated Feynman diagrammatic formalism. In this context, a considerable effort has been recently devoted to the analysis of generalized susceptibilities and two-particle vertex functions [20–24] beyond the standard textbook discussions, with a particular focus on their high-frequency asymptotics [25–27] and on their algorithmic treatments [28]. Considering the specific case of the physical interpretation of the local (on-site) two-particle formalism, interesting information was obtained in Ref. [29]. The Shiba transformation, which maps

the quantities of a model with local electrostatic repulsion $U > 0$ to those of a corresponding Hamiltonian with on-site attraction $U < 0$, was applied to derive the explicit relations between the on-site generalized two-particle susceptibilities of the repulsive Hubbard model and their counterparts in the attractive Hubbard model. In fact, the analytical derivations presented in Ref. [29] unveiled intrinsic symmetry properties of the four-point correlation functions (such as two-particle generalized susceptibilities and vertex functions) and provided pivotal information for the investigation of the breakdown of the self-consistent perturbation expansion in many-electron systems.

However, the analytical derivations of Ref. [29] were limited to a very specific case: the Shiba transformation of the static (i.e., for zero-frequency transfer, $\omega = 0$) two-particle generalized susceptibilities in the particle-hole symmetric Hubbard model, i.e., half-filling ($\mu = U/2$) and $SU(2)$ symmetry ($h = 0$). In this paper, our goal is to address and overcome these notable restrictions by providing the general expressions that systematically map all two-particle generalized on-site susceptibilities of a model with a purely local (Hubbard-like) interaction onto their counterparts in the corresponding model with sign-flipped interaction. Importantly, these mappings are established for arbitrary values of the chemical potential, applied magnetic field, and bosonic Matsubara frequency ω .

Eventually, to demonstrate the correctness and usefulness of the derived expressions, we validate them through a hands-on application. Specifically, we exploit these expressions to analyze the divergences affecting the irreducible two-particle vertex functions of the Hubbard atom (i.e., of an isolated interacting site) across different scattering sectors as a function of arbitrary chemical potential, magnetic field, temperature, and interaction. The obtained general phase diagrams will

*Contact author: herbert.essl@tuwien.ac.at

Published by the American Physical Society under the terms of the [Creative Commons Attribution 4.0 International license](https://creativecommons.org/licenses/by/4.0/). Further distribution of this work must maintain attribution to the author(s) and the published article's title, journal citation, and DOI.

provide an intuitive and robust guidance to all future studies aiming at unveiling the formal [30–33] and the physical [34–37] aspects associated with the breakdown [30–32] of the self-consistent perturbation theory for many-electron systems, *beyond* the (unrealistic) assumption of perfect particle-hole symmetry made so far in the largest part of the corresponding literature (with the notable exceptions of Refs. [33–35]).

The structure of the paper is as follows: In Sec. II, we concisely introduce the one- and two-particle formalism necessary for our derivations, and we recall the general definition of the Shiba transformation. In Sec. III, we report the explicit derivation for the mapping of generalized on-site two-particle quantities under the action of the Shiba transformation in the most general case (i.e., arbitrary filling, magnetic field, and finite transfer frequencies). Thereafter, in Sec. IV we apply the derived relations to the problem of the divergences of the irreducible vertex functions occurring in the different scattering channels of the Hubbard atom with repulsive and attractive interaction, whose specific study was hitherto restricted to the case of perfect particle-hole symmetry. Finally, in Sec. V we draw our conclusions, outlining possible consequences of the results presented in our work.

II. FORMALISM

A. Generalized susceptibilities

When examining the fermionic four-point correlation functions of systems that maintain time translation invariance, the associated generalized susceptibilities, which characterize the scattering events between two particles, depend only on three independent Matsubara frequencies (instead of four). This reduction is due to the conservation of energy [20,38]. Additionally, for spin conservation, only 6 out of the 2^4 spin combinations for these correlation functions remain independent [20].

Therefore, for our considerations all possible (local) generalized susceptibilities χ can be defined as follows [15,20]:

$$\begin{aligned} \chi_{\sigma\sigma'}(\nu_1, \nu_2, \nu_3) &= \int_0^\beta d\tau_1 d\tau_2 d\tau_3 e^{-i\nu_1\tau_1} e^{i\nu_2\tau_2} e^{-i\nu_3\tau_3} \\ &\times (\langle T_\tau c_\sigma^\dagger(\tau_1) c_\sigma(\tau_2) c_{\sigma'}^\dagger(\tau_3) c_{\sigma'}(0) \rangle \\ &- \langle T_\tau c_\sigma^\dagger(\tau_1) c_\sigma(\tau_2) \rangle \langle T_\tau c_{\sigma'}^\dagger(\tau_3) c_{\sigma'}(0) \rangle), \end{aligned} \quad (1)$$

$$\begin{aligned} \chi_{\sigma\sigma'}^-(\nu_1, \nu_2, \nu_3) &= \int_0^\beta d\tau_1 d\tau_2 d\tau_3 e^{-i\nu_1\tau_1} e^{i\nu_2\tau_2} e^{-i\nu_3\tau_3} \\ &\times \langle T_\tau c_\sigma^\dagger(\tau_1) c_{\sigma'}(\tau_2) c_{\sigma'}^\dagger(\tau_3) c_\sigma(0) \rangle, \end{aligned} \quad (2)$$

where σ, σ' denote the spins, ν_i are fermionic Matsubara frequencies (where the fourth frequency is set by $\nu_4 = \nu_1 - \nu_2 + \nu_3$), $c_\sigma^{(\dagger)}$ annihilate (create) an electron with spin σ , T_τ denotes the imaginary time ordering operator, and $\langle \dots \rangle = \frac{1}{Z} \text{Tr}(e^{-\beta H} \dots)$ is the thermal expectation value.

Note that for nonlocal χ , $c_{i,\sigma}^{(\dagger)}$ acquire an additional lattice index i , and for space translation invariant systems, one of the four lattice indices can be set to zero.

By using two fermionic ν , ν' , and one bosonic Matsubara frequency ω , one can define two convenient

frequency conventions: the particle-hole (ph) $\chi^{\nu,\nu',\omega}$ and the particle-particle (pp) $\chi_{\text{pp}}^{\nu,\nu',\omega}$ notation,

$$\text{ph: } \nu_1 = \nu, \quad \text{pp: } \nu_1 = \nu, \quad (3a)$$

$$\nu_2 = \nu + \omega, \quad \nu_2 = \omega - \nu', \quad (3b)$$

$$\nu_3 = \nu' + \omega, \quad \nu_3 = \omega - \nu, \quad (3c)$$

$$(\nu_4 = \nu'), \quad (\nu_4 = \nu'). \quad (3d)$$

One can go from ph to pp notation by shifting $\omega \rightarrow \omega - \nu - \nu'$.

Instead of using the definitions in (1) and (2) directly, it is often more useful to consider specific spin combinations, which correspond to physical response functions.

The spin combinations (channels) that we consider are charge (c), longitudinal spin (s), the coupling between charge and longitudinal spin (cs) and (sc), transversal spin ($S_x = S_y$), and the pairing channel (pair):

$$\chi_c^{\nu,\nu',\omega} = \chi_{\uparrow\uparrow}^{\nu,\nu',\omega} + \chi_{\downarrow\downarrow}^{\nu,\nu',\omega} + \chi_{\uparrow\downarrow}^{\nu,\nu',\omega} + \chi_{\downarrow\uparrow}^{\nu,\nu',\omega}, \quad (4)$$

$$\chi_s^{\nu,\nu',\omega} = \chi_{\uparrow\uparrow}^{\nu,\nu',\omega} + \chi_{\downarrow\downarrow}^{\nu,\nu',\omega} - \chi_{\uparrow\downarrow}^{\nu,\nu',\omega} - \chi_{\downarrow\uparrow}^{\nu,\nu',\omega}, \quad (5)$$

$$\chi_{cs}^{\nu,\nu',\omega} = \chi_{\uparrow\uparrow}^{\nu,\nu',\omega} - \chi_{\downarrow\downarrow}^{\nu,\nu',\omega} - \chi_{\uparrow\downarrow}^{\nu,\nu',\omega} + \chi_{\downarrow\uparrow}^{\nu,\nu',\omega}, \quad (6)$$

$$\chi_{sc}^{\nu,\nu',\omega} = \chi_{\uparrow\uparrow}^{\nu,\nu',\omega} - \chi_{\downarrow\downarrow}^{\nu,\nu',\omega} + \chi_{\uparrow\downarrow}^{\nu,\nu',\omega} - \chi_{\downarrow\uparrow}^{\nu,\nu',\omega}, \quad (7)$$

$$\chi_{S_x}^{\nu,\nu',\omega} = \chi_{S_y}^{\nu,\nu',\omega} = \chi_{\uparrow\downarrow}^{\nu,\nu',\omega} + \chi_{\downarrow\uparrow}^{\nu,\nu',\omega}, \quad (8)$$

$$\chi_{\text{pair}}^{\nu,\nu',\omega} = -\chi_{\uparrow\downarrow,\text{pp}}^{\nu,\nu',\omega} - (\chi_{\downarrow\uparrow,\text{pp}}^{\nu,\nu',\omega})^*. \quad (9)$$

For the subsequent discussion, it is convenient to view the generalized susceptibilities as (infinite-dimensional) matrices in the frequencies ν , ν' and treat ω as an additional parameter.

To simplify the notation, we are going to omit the fermionic frequencies ν and ν' in the following and state the bosonic frequency ω only explicitly when it is not the same for all quantities in an expression. Within this notation, all operations (e.g., multiplication, transposition, inversion, etc.) are meant as matrix operations in the fermionic Matsubara frequency space.

Note that for broken SU(2)-symmetry, the previously separate charge and the longitudinal spin channels get coupled into the longitudinal (L) channel

$$\chi_L = \begin{pmatrix} \chi_c & \chi_{cs} \\ \chi_{sc} & \chi_s \end{pmatrix}, \quad (10)$$

where the space of the longitudinal channel is a tensor product space of the charge and spin fermionic Matsubara frequency spaces.

The generalized susceptibility matrices show interesting properties that restrict their eigenvalues and eigenvector structure and depend on the symmetries of the considered model (see Appendix A for an in-depth discussion).

For $\omega = 0$, the matrices of the transversal spin channel χ_{S_x} as well as the pairing channel χ_{pair} can be identified as centro-Hermitian matrices [39] [see Eq. (A11)], and therefore only have eigenvalues that are real or come in complex-conjugate pairs [40]. Moreover, the matrix of the coupled longitudinal channel χ_L is classified as a κ -real matrix Eq. (A13), which shows the same eigenvalue properties [41].

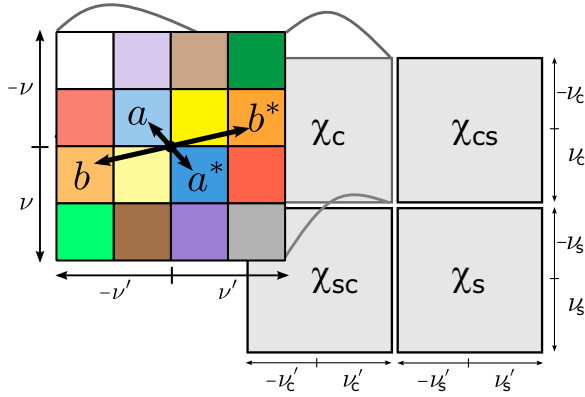


FIG. 1. Schematic illustration of a κ -real matrix that is built from blocks of centro-Hermitian matrices, which is relevant for the coupled longitudinal channel if $SU(2)_S$ -symmetry is violated.

In addition, the generalized susceptibilities for all considered channels are symmetric matrices and, hence, can be diagonalized by an orthogonal transformation [42]. This, together with the centro-Hermitian and κ -real property, respectively, leads to the fact that eigenvectors v_α corresponding to real eigenvalues λ_α have a symmetric/antisymmetric real part $\text{Re}v_\alpha$ (in ν) and an antisymmetric/symmetric imaginary part $\text{Im}v_\alpha$ [see Eq. (A16)] [39]. For the longitudinal channel, eigenvectors are symmetric/antisymmetric in the charge and spin subspace, respectively [see Eq. (A17)]. Figure 1 shows a schematic example of a κ -real matrix that is built from blocks of centro-Hermitian matrices in the fermionic Matsubara frequencies, as is the case in the coupled longitudinal channel.

A concise summary of the generalized susceptibility matrix properties for $\omega = 0$ in the different channels and under additional symmetries can be seen in Table I, where *No Symmetry* refers to time translation symmetry, spin conservation, and that the Hamiltonian is a real function of c and c^\dagger . Note that the last assumption can be violated, for example, by the inclusion of an external electromagnetic potential via the Peierls substitution in lattice models and/or if spin-orbit coupling is taken into account. All these symmetries can be derived by applying Eqs. (A6)–(A10) to the respective definitions of the different channels.

B. Shiba transformation

The mapping—we apply in this paper—systematically maps all quantities of a model with on-site interaction onto a corresponding model with sign-flipped interaction. It has been

used for the study in Ref. [29] and is derived by applying a partial (local) particle-hole transformation, or Shiba transformation [43], acting on the creation and annihilation operators with

$$c_\uparrow \rightarrow c_\uparrow, c_\uparrow^\dagger \rightarrow c_\uparrow^\dagger, c_\downarrow \rightarrow c_\downarrow^\dagger, \text{ and } c_\downarrow^\dagger \rightarrow c_\downarrow. \quad (11)$$

By considering a local single-orbital Hubbard Hamiltonian (written in a symmetric form with $\delta\mu = \mu - U/2$), one readily sees that applying the Shiba transformation

$$\begin{aligned} H(U, \delta\mu, h) &= \\ -\delta\mu(n_\uparrow + n_\downarrow) - h(n_\uparrow - n_\downarrow) + U(n_\uparrow - 1/2)(n_\downarrow - 1/2) & \\ \downarrow \text{Shiba} & \\ -\delta\mu(n_\uparrow - n_\downarrow) - h(n_\uparrow + n_\downarrow) - U(n_\uparrow - 1/2)(n_\downarrow - 1/2) & \\ = H(-U, h, \delta\mu) & \end{aligned} \quad (12)$$

($n_\sigma = c_\sigma^\dagger c_\sigma$) corresponds to interchanging the values of $\delta\mu \leftrightarrow h$ as well as a sign flip in the interaction U (any constant terms that appear from the mapping in the Hamiltonian have been omitted).

The Hamiltonian in Eq. (12) corresponds to the Hubbard atom (HA), which we consider for our exemplary study in Sec. IV for different fillings and external magnetic fields h . The model can be solved analytically [44]; the corresponding expressions for the one- and two-particle Green's functions can be found in Appendix D.

The (nonlocal) Shiba mapping can also be applied for a bipartite lattice model, i.e., a lattice that can be divided into two sublattices, where the hopping from each site only connects to the other sublattice. The Hamiltonian of such a Hubbard model (HM) reads

$$\begin{aligned} H &= - \sum_{i,j,\sigma} t_{ij} c_{i,\sigma}^\dagger c_{j,\sigma} - \delta\mu \sum_i (n_{i,\uparrow} + n_{i,\downarrow}) \\ &\quad - h \sum_i (n_{i,\uparrow} - n_{i,\downarrow}) + U \sum_i (n_{i,\uparrow} - 1/2)(n_{i,\downarrow} - 1/2), \end{aligned} \quad (13)$$

where t_{ij} is zero if i and j belong to the same sublattice. Assigning one sublattice to all even and the other one to all odd sites, respectively, we readily see that the nonlocal Shiba transformation $c_{i,\downarrow} \rightarrow c_{i,\downarrow}^\dagger (-1)^i$ leaves the hopping term Eq. (13) invariant and otherwise follows Eq. (12). Therefore, the effect of the Shiba transformation on bipartite

TABLE I. Matrix properties of the generalized susceptibilities under additional symmetries, where *No Symmetry* refers to time translation symmetry, spin conservation, and that the Hamiltonian is a real function of c and c^\dagger . For the additional symmetries, we use $SU(2)_S$ for Spin $SU(2)$ symmetry ($h = 0$), $SU(2)_P$ for pseudospin $SU(2)$ symmetry ($\delta\mu = 0$), PH for particle-hole symmetry [$SU(2)_S$ and $SU(2)_P$ symmetry].

Symmetry	$\chi_L^{\omega=0}$	$\chi_{Sx}^{\omega=0}$	$\chi_{\text{pair}}^{\omega=0}$
No symmetry	κ -real, symmetric	centro-Hermitian, symmetric	centro-Hermitian, symmetric
$SU(2)_S$	block-diagonal, κ -real, symmetric	centro-Hermitian, symmetric	bisymmetric, real
$SU(2)_P$	κ -real, symmetric	bisymmetric, real	centro-Hermitian, symmetric
PH [$SU(2)_S \otimes SU(2)_P$]	block-diagonal, real, symmetric	bisymmetric, real	bisymmetric, real

systems (with local on-site interaction) can be regarded to be analog to purely local systems.

The Shiba mapping is linked to two sets of SU(2) spin algebras, of which the generators are the (local) spin operator \mathcal{S} with the components

$$\mathcal{S}_x = c_{\uparrow}^{\dagger}c_{\downarrow} + c_{\downarrow}^{\dagger}c_{\uparrow}, \quad (14)$$

$$\mathcal{S}_y = -i(c_{\uparrow}^{\dagger}c_{\downarrow} - c_{\downarrow}^{\dagger}c_{\uparrow}), \quad (15)$$

$$\mathcal{S}_z = c_{\uparrow}^{\dagger}c_{\uparrow} - c_{\downarrow}^{\dagger}c_{\downarrow} \quad (16)$$

and the (local) pseudospin operator \mathcal{S}_p with the components

$$\mathcal{S}_{p,x} = c_{\uparrow}^{\dagger}c_{\downarrow}^{\dagger} + c_{\downarrow}c_{\uparrow}, \quad (17)$$

$$\mathcal{S}_{p,y} = -i(c_{\uparrow}^{\dagger}c_{\downarrow}^{\dagger} - c_{\downarrow}c_{\uparrow}), \quad (18)$$

$$\mathcal{S}_{p,z} = c_{\uparrow}^{\dagger}c_{\uparrow} + c_{\downarrow}^{\dagger}c_{\downarrow} - 1. \quad (19)$$

Evidently, the Shiba transformation maps the spin \mathcal{S} to the pseudospin \mathcal{S}_p . Since the components of \mathcal{S} and \mathcal{S}_p commute, spin and pseudospin can be regarded as independent set of operators [38].

The pseudospin can be given the following physical interpretation: $\mathcal{S}_{p,x}$ and $\mathcal{S}_{p,y}$ correspond to the local Cooper pair operators, which describe the real and imaginary part of the order parameter of a strong-coupling (Bose-Einstein-like) superconductor, and $\mathcal{S}_{p,z}$ describes the deviation of the density from half-filling.

The Hamiltonian in the upper line of in Eq. (12) commutes with all components of \mathcal{S} if $h = 0$, which we will denote as SU(2)_S symmetry, and with all components of \mathcal{S}_p for $\delta\mu = 0$, referred to as SU(2)_P symmetry.

Systems that exhibit a symmetry under rotations generated by spin *and* pseudospin are symmetric under SO(4) \simeq [SU(2)_S \otimes SU(2)_P]/ \mathbb{Z}_2 [38]. These SO(4) symmetric systems are particle-hole symmetric [45].

The on-site physical susceptibilities, describing the (linear) response of the system on a local observable A when a local observable B is coupled to an external perturbation, can be calculated by Fourier-transforming/analytically continuing the following expression:

$$\chi_{AB}^{\text{phys}}(\tau) = \langle A(\tau)B(0) \rangle - \langle A \rangle \langle B \rangle. \quad (20)$$

In Matsubara frequency space, they are related to the generalized susceptibilities via

$$\chi_r^{\text{phys}}(\omega) = \frac{1}{\beta^2} \sum_{vv'} \chi_r^{vv'\omega}. \quad (21)$$

Using Eq. (21) and the definitions in Eqs. (4)–(9), we find

$$\chi_c^{\text{phys}} : A = B = \mathcal{S}_{p,z}, \quad (22)$$

$$\chi_s^{\text{phys}} : A = B = \mathcal{S}_z, \quad (23)$$

$$\chi_{cs}^{\text{phys}} : A = \mathcal{S}_{p,z}, B = \mathcal{S}_z, \quad (24)$$

$$\chi_{sc}^{\text{phys}} : A = \mathcal{S}_z, B = \mathcal{S}_{p,z}, \quad (25)$$

$$\chi_{S_x}^{\text{phys}} : A = B = \mathcal{S}_x, \quad (26)$$

$$\chi_{\text{pair}}^{\text{phys}} : A = B = \mathcal{S}_{p,x}. \quad (27)$$

The mapping of the physical susceptibilities under the Shiba transformation is thereby clearly identified from

the corresponding mapping of the spin and pseudospin components.

The more complicated case of the Shiba mapping for the local generalized susceptibilities is derived in Sec. III.

III. DERIVATION OF THE MAPPING

In the following, we derive how the Shiba transformation in Eq. (11) is acting on the local [46] generalized susceptibilities of the charge, longitudinal spin, transversal spin, and pairing channel [see Eqs. (4)–(9)] for the most general cases, i.e., arbitrary filling, external magnetic field, and arbitrary bosonic transfer frequency ω . Thereby, the coupling of the charge and longitudinal spin channel for broken SU(2)_S symmetry, i.e., finite magnetic field h , into the longitudinal channel [cf. Eq. (10)] has to be explicitly considered.

By applying the Shiba transformation on the general definition in Eq. (1), we find the relations

$$\begin{aligned} \chi_{\uparrow\uparrow,U}^{v,v',\omega} &= \chi_{\uparrow\uparrow,-U}^{v,v',\omega}, & \chi_{\downarrow\downarrow,U}^{v,v',\omega} &= \chi_{\downarrow\downarrow,-U}^{-v-\omega,-v'-\omega,\omega}, \\ \chi_{\uparrow\downarrow,U}^{v,v',\omega} &= -\chi_{\uparrow\downarrow,-U}^{v,-v'-\omega,\omega}, & \text{and } \chi_{\downarrow\uparrow,U}^{v,v',\omega} &= -\chi_{\downarrow\uparrow,-U}^{-v-\omega,-v',\omega}, \end{aligned} \quad (28)$$

where the subscript U refers to the model parameters ($U, \delta\mu, h$) and the subscript $-U$ to $(-U, h, \delta\mu)$, i.e., the two models related by the Shiba transformation in Eq. (12).

With these building blocks, we can now apply the Shiba mapping to the coupled longitudinal channel. We start with the case of $\omega = 0$ and then generalize to finite bosonic frequencies.

We will identify the similarity transformation S that captures the action of the Shiba transformation onto the generalized susceptibilities $\chi_{L,U}$ and $\chi_{L,-U}$. Thereby, we employ the following matrix Q in Matsubara space:

$$Q = \frac{1}{\sqrt{2}} \begin{pmatrix} \mathbb{1} & -J \\ \mathbb{1} & J \end{pmatrix} \quad \text{with } J = \begin{pmatrix} & 1 \\ \cdot & \\ 1 & \end{pmatrix}, \quad (29)$$

where we divided the Matsubara frequencies into quadrants of positive + and negative – frequencies

$$\begin{pmatrix} \chi^{--} & | & \chi^{+-} \\ \chi^{+-} & | & \chi^{++} \end{pmatrix}. \quad (30)$$

The similarity transformation $Q^T \chi_{CS} Q$ separates the symmetric and antisymmetric part of a centrosymmetric matrix ($JAJ = A$) into two blocks along the diagonal, and the symmetric and antisymmetric part of a centro-skew-symmetric matrix ($JAJ = -A$) into two blocks along the skew diagonal.

Hence, a similarity transformation with Q separates the real χ' and imaginary part χ'' of a centro-Hermitian matrix χ_{CH} ($J\chi_{CH}J = \chi_{CH}^*$) into the symmetric and antisymmetric components, respectively,

$$Q\chi_{CH}Q^T = \begin{pmatrix} \chi'_A & i\chi''_S \\ i\chi''_A & \chi'_S \end{pmatrix}. \quad (31)$$

A detailed definition of the different blocks can be found in Appendix C.

By defining the transformations Q and T in the tensor product space of the coupled L channel,

$$Q = \begin{pmatrix} Q & 0 \\ 0 & Q \end{pmatrix} \quad \text{and} \quad T = \begin{pmatrix} \mathbb{1} & 0 & 0 & 0 \\ 0 & 0 & 0 & \mathbb{1} \\ 0 & 0 & \mathbb{1} & 0 \\ 0 & \mathbb{1} & 0 & 0 \end{pmatrix} \quad (32)$$

[cf. Eq. (10)], we can determine (see Appendix C) the transformation S , which relates the two sides of the Shiba transformation:

$$\chi_{L,U} = S \chi_{L,U} S \quad \text{with} \quad S = Q^T T Q. \quad (33)$$

In Appendix C we show that this relation holds for arbitrary bosonic transfer frequencies ω , when adapting the Q and T matrices by shifting the boundaries of the Matsubara frequency quadrants by $(-\omega/2, -\omega/2)$ in analogy to Eq. (30).

Hence, for finite ω the susceptibility matrices can be viewed as centro-Hermitian in regard to the shifted Matsubara frequency basis [see Eq. (A12)].

From Eq. (33) [more visible in Eq. (C14)] it follows that the Shiba transformation leaves the real antisymmetric part χ'_A of each charge-spin component ($\chi_c, \chi_s, \chi_{cs}, \chi_{sc}$) in χ_L invariant and exchanges the real symmetric part χ'_S between $\chi_c \leftrightarrow \chi_s$ and between $\chi_{cs} \leftrightarrow \chi_{sc}$,

$$\begin{aligned} \chi'_{c,-U,A} &\longleftrightarrow \chi'_{c,U,A}, \\ \chi'_{s,-U,A} &\longleftrightarrow \chi'_{s,U,A}, \\ \chi'_{c,-U,S} &\longleftrightarrow \chi'_{c,U,S}, \\ \chi'_{cs,-U,A} &\longleftrightarrow \chi'_{cs,U,A}, \\ \chi'_{sc,-U,A} &\longleftrightarrow \chi'_{sc,U,A}, \\ \chi'_{cs,-U,S} &\longleftrightarrow \chi'_{sc,U,S}. \end{aligned} \quad (34)$$

For the imaginary parts, neither the symmetric nor the antisymmetric part is invariant under the mapping, and they exchange according to the rules below:

$$\begin{aligned} \chi''_{cs,-U,A} &\longleftrightarrow \chi''_{s,U,A}, \\ \chi''_{sc,-U,A} &\longleftrightarrow \chi''_{c,U,A}, \\ \chi''_{c,-U,S} &\longleftrightarrow \chi''_{cs,U,S}, \\ \chi''_{sc,-U,S} &\longleftrightarrow \chi''_{s,U,S}. \end{aligned} \quad (35)$$

By examining the eigenvectors of the generalized susceptibility in the longitudinal channel, it follows that the symmetric part in one subspace is mapped from the charge to the spin subspace, and vice versa. However, the antisymmetric part remains unaffected by this transformation [refer to Eqs. (C18) and (C19)].

Finally, we apply the Shiba transformation on the generalized susceptibilities of the pairing and the transversal spin channel. From the transformation of Eq. (2) we get

$$\chi_{S_x,U}^\omega = \chi_{\text{pair},U}^{-\omega} \quad (36)$$

(details are in Appendix C).

IV. APPLICATION OF THE MAPPING

The mapping derived in Sec. III can be useful in several practical contexts, being applicable also beyond the purely local Hubbard atom Hamiltonian in the first line of Eq. (12).

In fact, the expressions derived in the previous section may also be applied to the local two-particle quantities of bipartite lattice models with on-site electrostatic interaction, where their mapping would work in a completely analogous fashion [see Eq. (13)]. For instance, our equations could be directly exploited to map the on-site generalized susceptibilities of the Hubbard model on a generic d -dimensional bipartite lattice with nearest-neighbor [47] hopping t and $(U, \delta\mu, h)$ to the corresponding lattice model with the same hopping and $(-U, h, \delta\mu)$ [48]. Evidently, this feature renders the derived mapping also immediately applicable to the local two-particle quantities of the widely used dynamical mean-field theory (DMFT) [49].

Independent of the specific models considered, an evident advantage of the mapping is to potentially reduce the effort of two-particle calculations if these need to be systematically performed in different regions of the phase diagram. Further, one could exploit the mapping to investigate the two-particle properties of regimes [e.g., with $SU(2)_S$ -broken symmetry] that might otherwise not be directly and/or easily accessible with the numerical algorithms at our disposal.

Finally, the derived mapping gives also some fundamental insights on how two-particle quantities of different scattering channels are connected to each other and how they are linked to the symmetries of the system.

As an example to illustrate how this aspect of the mapping works, we look at the problem of the two-particle irreducible vertex divergences in the Hubbard atom, which is of considerable interest in the context of the investigation of the breakdown of the self-consistent perturbation expansion for many-electron systems.

A. Vertex divergences and their generalization

In this section, we extend the existing studies [22,29,32,50] on the divergences in the two-particle irreducible vertex of the Hubbard atom, which have been hitherto restricted to the rather specific, highly symmetric case of $\delta\mu = h = 0$ [i.e., of perfect particle-hole symmetry, so $SU(2)_S$ and $SU(2)_P$ symmetry]. In particular, we aim here at individuating the divergences of the two-particle irreducible vertices at transfer frequency $\omega = 0$ in all scattering channels for the *whole* parameter space of the Hubbard atom with positive (repulsive) as well as negative (attractive) on-site interaction, arbitrary filling, and in the presence of an external magnetic field h .

We briefly recall here that the two-particle irreducible vertex function $\Gamma_r^{v,v'}(\omega)$ in a given scattering channel r (e.g., longitudinal, pairing, etc.) is formally defined [20,38,51,52] as the kernel of the (self-consistent) Bethe-Salpeter equation (BSE) in the corresponding sector r , and, as such, it can be computed by inverting the BSE, i.e.,

$$\Gamma_r^{v,v'}(\omega) := [\chi_r^{-1}]^{v,v',\omega} - [\chi_{r,0}^{-1}]^{v,v',\omega},$$

where the transversal channel has to be treated with care if $H \notin \mathbb{R}$ and $\omega \neq 0$ (see Appendix B).

Hence, the divergences of the Γ_r are directly determined by the vanishing of an eigenvalue of the corresponding generalized susceptibility matrix $\chi_r^{v,v',\omega}$ in the fermionic Matsubara frequencies v, v' [53].

As mentioned in Sec. II A by perfect $SU(2)_S$ and $SU(2)_P$ symmetry, all local two-particle quantities for zero-transfer

frequency ($\omega = 0$) are real and symmetric matrices. Hence, the *sign change* of an eigenvalue can only happen if this eigenvalue vanishes. This eigenvalue is then responsible for the divergence of $\Gamma_r^{v'v}$. These sign changes, as discussed in the recent literature [29,32,35–37,54], are crucial to drive the suppression/enhancements of the corresponding physical static response of the systems, and, in more complicated lattice systems, even to trigger thermodynamic phase-instabilities [35,39,54–57]. However, if either $SU(2)_S$ ($h \neq 0$) or $SU(2)_P$ ($\delta\mu \neq 0$) symmetries are broken, $\chi_r^{v'v}$ no longer has to be a real and symmetric matrix for all channels, but it can be either a centro-Hermitian or a κ -real matrix (see Table I). Consequently, its eigenvalues are no longer required to be real: They can be either real or appear in complex-conjugate pairs, consistent with the fundamental theorem of algebra [40,41].

As a consequence, the discussed sign changes of an eigenvalue of the generalized susceptibilities, or at least of their real part, may now occur continuously in the parameter space *without* the necessity that the eigenvalue vanishes, which would trigger a vertex divergence. In fact, complex-conjugate pairs of eigenvalues can switch the sign of their real parts without vanishing by keeping their imaginary parts finite. We note that the occurrence of this specific behavior of the eigenvalues of the generalized charge susceptibility has been reported in the phase diagram of Ref. [33] showing the DMFT [49]/cellular-DMFT [58,59] solution of the HM out of half-filling, as well as, in a somewhat different perspective, in Refs. [35,39,56]. Indeed, these observations highlight the general relevance of such an evolution of the eigenvalues of the generalized susceptibility beyond the specific framework of the HA, which we are going to investigate systematically in the following. In this context, we define the occurrence of a complex-conjugate pair of eigenvalues with a vanishing real part but a finite imaginary part as *pseudodivergence*. In this way, the concept of vertex divergences can be extended to those cases in which sign changes of the real part of an eigenvalue pair of $\chi_r^{v'v}$ are not directly associated with an actual divergence of $\Gamma_r^{v'v}$. Loosely speaking, this generalization might recall the case of a branch cut of the square root function, which is not crossing through the origin but rather the negative real axis at a finite value by changing the sign of the imaginary part. Eventually, the pseudodivergences defined here in the physical parameter space may be linked to the analytic properties of the generalized susceptibilities [60,61] and/or of the perturbative expansion of the electron self-energy [10,62–64] in abstract complex planes obtained, e.g., through the complexification of the electronic interaction U [10,60,61].

B. Dimensionless representation

Before starting the analysis of the vertex divergences and pseudodivergences in the whole phase space of the Hubbard atom, it is convenient to make a general consideration based on the formal Lehmann representation of the on-site [65] generalized susceptibilities, whose expressions are reported, e.g., in Appendix D and Ref. [66]. To obtain a dimensionless representation, we scale all parameters of the Hamiltonian with inverse temperature β . Formally, this can be done by

considering a model Hamiltonian, which is defined through N real parameters $\{\varepsilon_i\}_{i=1}^N$ (e.g., the hopping t , the on-site interaction U , etc.), where all ε_i have the dimension of an energy. Evidently, all eigenenergies of the many-electron Hamiltonian considered will only depend on these parameters (or a combination thereof), i.e., $\{E_j\} = \{E_j(\{\varepsilon_i\})\}$. As a consequence, all corresponding dimensionless quantities βE_j must only be dependent on the set $\{\beta\varepsilon_i\}$ for all j . Then, by looking at the Lehmann representation of the generalized susceptibility, one readily realizes that, apart from an overall scaling of β^3 , the generalized susceptibility can always be expressed in terms of the parameter set $\{\beta E_j\}$, which can be fully expressed via the parameter set $\{\beta\varepsilon_i\}$. Therefore, one can rewrite the Lehmann representation as

$$\chi_{\alpha_1, \alpha_2, \alpha_3, \alpha_4}^{v'v\omega}(\beta, \{\varepsilon_i\}) = \beta^3 f_{\alpha_1, \alpha_2, \alpha_3, \alpha_4}^{nm'm}(\{\beta\varepsilon_i\}), \quad (37)$$

where n, n' and m are the indices for v, v' and ω , and α_i is a generic set of quantum numbers. On the basis of this observation, presenting our results for the location and the properties of the vertex (pseudo)divergences of the HA in the *dimensionless* parameter space $\{\beta\delta\mu, \beta h, \beta U\}$ turns out to be a particularly convenient choice, as it allows for a “universal” representation of our findings, directly applicable to any finite value of the temperature.

Before discussing the results, let us clarify the semantics. The nature of the vertex (pseudo)divergence is made clear by the color and the line-style in the plot: Solid lines mark divergences and dashed lines mark pseudodivergences. For identifying the different channels where the (pseudo)divergence occurs, we adopt the following color-coding, extending the one introduced in the existing literature: We use *red* for a vertex (pseudo)divergence in the charge channel; *yellow* for the pairing channel; *green* for the longitudinal spin channel; *blue* for the transversal spin channel; and *bluish green* for the spin channel at $SU(2)_S$ symmetry, where all three spin directions are equivalent. Eventually, for broken $SU(2)_S$ symmetry ($h \neq 0$), where the coupled longitudinal channel needs to be considered as a whole, a weighted mixing of green and red is used. The proportion of red/green is determined by the percentage of the norm that the vector has in the charge/spin subspace. For more information, see Appendix E. Further, we classify a divergence as “symmetric/antisymmetric” if the corresponding eigenvector of the generalized susceptibility, which has a vanishing eigenvalue, has a symmetric/antisymmetric real part and an antisymmetric/symmetric imaginary part, provided that we use the norm Eq. (A15) to normalize the eigenvectors.

C. Vertex divergences of the HA: Limiting cases

We start our analysis by illustrating in Fig. 2 the results obtained for two selected planes in the dimensionless phase space introduced above. These correspond to the two special cases beyond perfect particle-hole/SO(4) symmetry, where either the $SU(2)_S$ [$h = 0$, Fig. 2(a)] or the $SU(2)_P$ [$\delta\mu = 0$, Fig. 2(b)] symmetry is preserved. Such a choice allows us to showcase in the most transparent way the action of the Shiba-mapping on the vertex functions beyond particle-hole symmetry. In fact, a first glance at the geometrical shape and at the nature (encoded by the different colors) of the

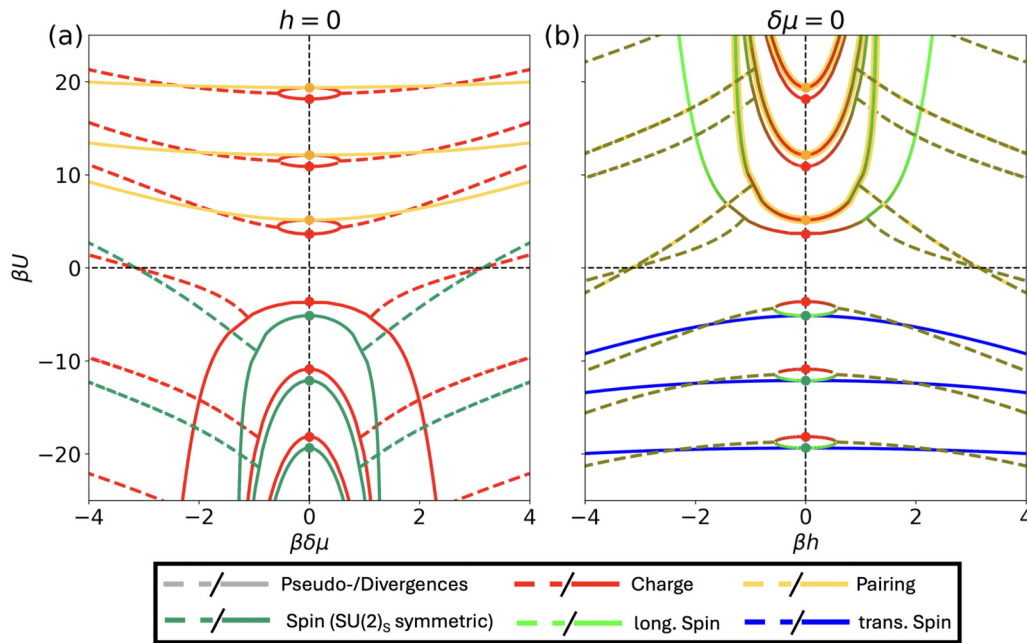


FIG. 2. Dimensionless phase space diagram of the Hubbard atom with repulsive and attractive interaction, showing the location and the nature of the (pseudo)divergences of the irreducible vertex functions in the different channels for the two special cases of (a) no magnetic field but out of half-filling (left panel), and (b) half-filling in the presence of a magnetic field (right panel). Solid lines mark divergences, and dashed lines mark pseudodivergences, while in order to identify the different channels, the following color coding is adopted (see the legend in the box below the figure): *red* for a vertex (pseudo)divergence in the charge channel; *yellow* for the pairing channel; *green* for the longitudinal spin channel; *blue* for the transversal spin channel; *bluish green* for degenerated spin channel. Further, when $SU(2)_S$ symmetry is broken ($h \neq 0$), the coupled longitudinal channel needs to be considered as a whole (see the text): In this case, a weighted mixing of green and red has been used.

vertex (pseudo)divergence lines displayed in Fig. 2 easily unveils the direct connection between the results of the repulsive model for varying $\delta\mu$ [upper panel of Fig. 2(a)] and those of the attractive model for varying h [lower panel of Fig. 2(b)]. Consistent with the mapping relations, an analogous correspondence is also observed between our two-particle calculations for the attractive model at different $\delta\mu$ [lower panel of Fig. 2(a)] and those for the repulsive model at different h [upper panel of Fig. 2(b)].

Before proceeding with the detailed analysis of the geometry and the nature of vertex (pseudo)divergence lines in Fig. 2, we recall that for the case of perfect particle-hole/ $SO(4)$ symmetry ($\delta\mu = h = 0$), it has been analytically demonstrated in the literature [22,29,50] that the HA displays a discrete set of vertex divergences, marked by colored dots in Fig. 2. In particular, for $U > 0$, the red dots on the positive βU -axis of both panels of Fig. 2 indicate the location of the irreducible vertex divergences in the charge channel of the HA associated with an antisymmetric eigenvector, while the orange dots mark the simultaneous occurrence of vertex divergences in the charge and in the pairing sector, associated with a symmetric eigenvector. Consistent with the mapping for perfect particle-hole symmetry [29], one finds along the negative βU axes of Fig. 2, exactly in mirrored positions with respect to the $U > 0$ case, alternating antisymmetric vertex divergences in the charge sector (red dots) and symmetric ones in the spin sector (bluish green dots).

We begin now our detailed discussion of the vertex divergences in the HA beyond particle-hole symmetry by

examining the data shown in Fig. 2(a), corresponding to the case of $h = 0$ and varying $\delta\mu$. Here, it should be stressed that, as soon as the $SU(2)_p$ -symmetry is lifted for any $\delta\mu \neq 0$, the symmetric divergences in the charge and pairing channel, marked by the orange dots on the positive βU axes of Fig. 2, no longer occur simultaneously, yielding separate divergence lines (marked in yellow and red, respectively, for the pairing and the charge sector). However, this is not the only qualitative difference emerging between these two kinds of vertex divergences for $\delta\mu \neq 0$: As reported in Table I, the generalized susceptibility in the pairing channel is a real and bisymmetric matrix as long as the $SU(2)_S$ symmetry is preserved. Therefore, differently from its charge counterpart, its eigenvalues remain purely real numbers, and the associated vertex actually diverges, without any possible occurrence of pseudodivergences and/or exceptional points (EPs). The latter are defined as the points in parameter space where two (or more) eigenvalues *and* eigenvectors coalesce and the matrix is no longer diagonalizable [39,42]. For the same reason, the symmetric nature of its singular eigenvectors is maintained for arbitrary values of $\delta\mu$.

On a more geometrical viewpoint, one can easily observe in Fig. 2(a) that the divergence lines of the charge sector form elliptic-shaped loops in the phase space, terminating on both sides in EPs for positive and negative values of $\delta\mu$. Henceforth, for the sake of conciseness, we will refer to these specific divergence structures, including the associated pseudodivergence lines, with the short-hand term of *loops*. These loops each consist of one symmetric (upper loop part)

and one antisymmetric (lower loop part) divergence line that meet at an EP. From this EP, a pseudodivergence line emerges. Quantitatively, we note that the EPs of the loop found at the lowest βU values correspond to a hole/electron doping of about 6%, which roughly coincides [67] with the doping level at which the corresponding EPs have been found in the DMFT/cellular DMFT calculations of the HM of Ref. [33]. It is also important to stress that the three loops shown in Fig. 2, just like all the other vertex-divergence structures discussed in the following, represent only the first three loop structures encountered by increasing βU . In fact, consistent with Refs. [22,50,68], where the occurrence of infinitely many vertex divergences at half-filling has been demonstrated, we also find infinitely many loops for increasing βU values.

Turning now to the study of the attractive sector, we find that the divergence lines show a completely different shape: They are disposed in a series of parabolas one inside the other, as can be seen in the bottom part of Fig. 2(a). More specifically, considering first the charge sector, the geometrical maximum of the parabola is represented by the (antisymmetric) divergences located at particle-hole symmetry. Upon doping, an antisymmetric divergence line meets with a symmetric divergence line out of half-filling at an EP, forming a pseudodivergence line. The qualitatively different geometrical structure compared to the elliptical-shaped divergence line structures in the repulsive sector corresponds to a specific difference: Each symmetric divergence line extends down to $\beta U \rightarrow -\infty$. The reason why this happens is the absence of symmetric divergences at half-filling in the charge sector, which prevents the formation of closed loops of symmetric/antisymmetric divergences, in contrast with the repulsive sector.

In the spin sector, we observe an analogous situation [69], only with interchanged roles of the eigenvector symmetries: The symmetric divergence lines, originating from the corresponding purely symmetric divergences at half-filling, meet with an antisymmetric divergence line, extended down to $\beta U \rightarrow -\infty$, at an EP, from which a pseudodivergence emerges.

A second important difference with respect to the repulsive case is represented by the orientation of the pseudodivergences of both channels. These, after emerging from the corresponding EPs, are directed towards *smaller* absolute values of βU , in contrast with the pseudodivergences in the repulsive sector. Even more remarkably, they do cross the $U = 0$ axis, continuing afterwards in the repulsive sector. Hence, one may regard the pseudodivergences lines that cross the $U = 0$ axis as driven by the symmetry-breaking fields ($\delta\mu$ and/or h) in contrast to the pseudodivergences lines that do not cross the $U = 0$ axis, which would then be driven by the interaction U . More specifically, one can classify the (pseudo)divergences with an integer number N identifying the positive Matsubara frequency at which their associated eigenvector displays its largest component. In this way, we find that the N th pseudodivergence of both channels crosses the $U = 0$ axis at $\beta\delta\mu = \beta\mu = \pm(2N - 1)\pi$ (see Appendix G). In fact, this has to be the same point, because the generalized susceptibilities of two channels coincide for $U = 0$, due to the absence of vertex corrections. For more detailed information, see [70].

As we noted at the beginning of this subsection, in the case of preserved $SU(2)_P$ symmetry [i.e., $\delta\mu = 0, h \neq 0$; see Fig. 2(b)], the mapping relations determine a perfectly “mirrored” disposition of vertex divergences and pseudodivergences, with the parabola structures now located in the repulsive sector and the loop structure in the attractive one.

At the same time, as $SU(2)_S$ symmetry is broken for $h \neq 0$, the spin channel splits in the spin transverse (blue lines) channel and in the spin longitudinal channel (green lines), whereas the latter becomes coupled to the charge one (red) in what we have defined as the longitudinal sector. In particular, consistent with the mapping, all pairing vertex divergences in the repulsive sector of the $SU(2)_S$ case [yellow lines in Fig. 2(a)] are transformed in the corresponding divergences of the transversal channel in the attractive sector with $SU(2)_P$ symmetry [blue lines in Fig. 2(b)]. Indeed, for the same reasons explained above, the generalized susceptibility of the spin transversal channels remains real and bisymmetric for $\delta\mu = 0$ when the $SU(2)_P$ symmetry is preserved. Analogously, all the loop and the parabola structures define now divergences in the combined longitudinal sector, whereas the specific ratio between their components in the charge and spin longitudinal subspaces is highlighted by the red/green color scale [71], as detailed in Appendix E. Moreover, a parabola in the pairing channel [marked by a thicker yellow line in Fig. 2(b)] is superimposed to every second parabola of divergences in the longitudinal sector.

D. The $T = 0$ limit

Before coming to the study of the most general case, where both $SU(2)_S$ and $SU(2)_P$ are violated, it is worthwhile to exploit our results to infer how the vertex (pseudo)divergences evolve in the $T \rightarrow 0$ limit. In fact, in spite of its intrinsic interest (e.g., to discuss the relation between the breakdown of self-consistent perturbation theory and the possible violation of the Luttinger theorem), most of the analysis of the nonperturbative effects on the two-particle level have been restricted to the finite- T case. The choice of working in dimensionless phase space offers a valuable opportunity to fill this gap, at least for the HA. Indeed, although our temperature-independent representation of the vertex divergences can be used, strictly speaking, only to analyze finite- T cases, the possibility of systematically extracting information for arbitrarily small temperatures and evaluating the asymptotic behavior of vertex (pseudo)divergence lines allows for a description of the $T = 0$ limit.

The results obtained are summarized in the schematic representation of the $T = 0$ phase space, Fig. 3, while more details about the procedure used can be found in Appendix F.

In particular, in the lower panels of Fig. 3 we observe a *continuous* distribution of vertex divergences at particle-hole symmetry ($\delta\mu = h = 0$), which occur in the charge and pairing (spin) channels for $U > 0$ ($U < 0$). The continuity of the vertex divergence distribution at $T = 0$ evidently reflects the continuity of the Matsubara frequencies in that limit, and appears consistent with the increasingly dense structure of the finite- T divergences reported (but not explicitly discussed) in previous works at particle-hole symmetry [22,29,50].

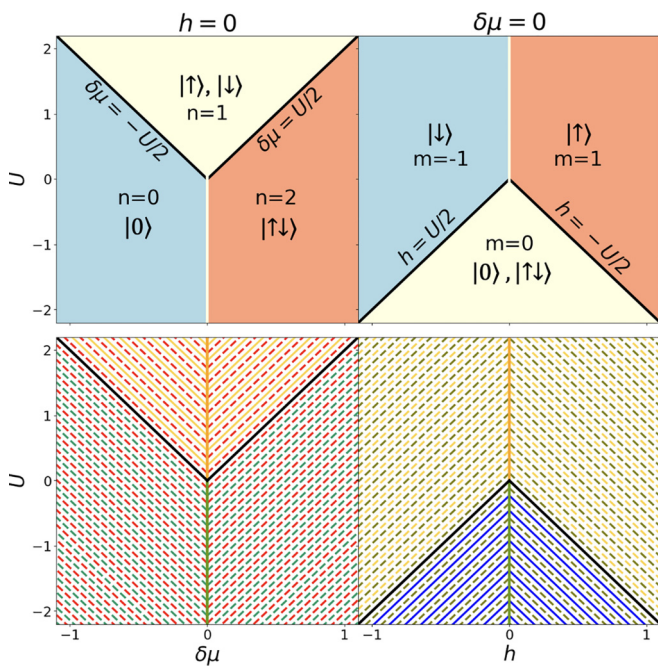


FIG. 3. Schematic phase space diagram of the vertex (pseudo)divergences (bottom panels) in the Hubbard atom at $T = 0$ for the two special cases shown in Fig. 2 (left: $h = 0$ and $\delta\mu \neq 0$; right: $h \neq 0$ and $\delta\mu = 0$) compared to the corresponding filling $n = n_{\uparrow} + n_{\downarrow}$ (upper left) and magnetization $m = n_{\uparrow} - n_{\downarrow}$ (upper right) of the system. These values can be understood by the corresponding ground state(s) of the HA, which are explicitly depicted in the different parameter regions. This schematic phase space diagram should be understood as a continuous distribution of (pseudo)divergences of a different nature in the whole phase space of the HA at $T = 0$: A divergence or pseudodivergence of the vertex is found at every point in the phase space, whereas the channel in which it occurs is encoded by the color of the dense set of lines shown in the bottom panels. The plotting conventions are as in Fig. 2.

Of greater interest are the results *out of particle-hole symmetry*. In particular, for $h = 0$ (lower left in Fig. 3), we observe a V-shaped area in the $U > 0$ sector (marked by black lines in Fig. 3) located between $\delta\mu = -U/2$ and $\delta\mu = U/2$, which corresponds to the regime of the HA where the ground state is half-filled (see the upper left in Fig. 3). Remarkably, for *every* parameter set within this V-shaped area, a vertex divergence in the pairing channel and pseudodivergence in the charge channel are found simultaneously. Indeed, the latter ones stem from the “looplike” structures in Fig. 2(a), which collapse on the $\delta\mu = 0$ axis in the $T = 0$ limit. Outside the V-shaped area, i.e., in the region that corresponds to a totally empty or totally full ground state for all U (see the upper left in Fig. 3), we find the occurrence of simultaneous pseudo-divergences in the spin and the charge channel everywhere (see Fig. 3, lower left). The pseudodivergences originate from the parabola structures in Fig. 2(a) as they progressively move towards the $\delta\mu = 0$ axis in the $U < 0$ sector.

In the opposite situation of $\delta\mu = 0$ (lower right panel in Fig. 3) we find, as expected, a “mirrored” distribution of divergences and pseudodivergences: the V-shaped region is now located in the $U < 0$ sector, between $\delta\mu = -U/2$ and

$U/2$. At the same time, due to the violation of the $SU(2)_S$ symmetry and in accordance with the mapping, the V-shaped region entails maximally mixed pseudodivergences in the longitudinal sector and divergences in the transversal spin channel, while pseudodivergences in the longitudinal and pairing channel are present outside.

E. Vertex divergences of the HA: The general case

We turn eventually to a discussion of the vertex divergences of the HA in the general case, i.e., for arbitrary values of h and $\delta\mu$. For the sake of compactness, we introduce the parameters α and r , as sketched in Fig. 4(b), in order to facilitate the visualization of our results when the values of $\delta\mu, h$ are varied between the limiting cases of $h = 0$ ($\alpha = 0$) and $\delta\mu = 0$ ($\alpha = 90^\circ$) shown in Figs. 2(a) and 2(b), respectively.

Specifically, the parameters α and r are defined as the following set of cylinder coordinates:

$$\delta\mu = r \cos \alpha \quad \text{and} \quad h = r \sin \alpha. \quad (38)$$

It is then easy to see that the sets of $\delta\mu, h$ values connected by the mapping linking the attractive and the repulsive model, according to Eq. (12), correspond to this simple relation for the polar coordinate α :

$$\alpha \leftrightarrow \alpha' \quad \text{with} \quad \alpha + \alpha' = 90^\circ, \quad (39)$$

whereas r remains unchanged.

Further, due to Eqs. (A3)–(A5), it is enough to consider $\alpha \in [0^\circ, 90^\circ]$, as all other regions of the phase space can be reconstructed from this interval.

In Fig. 4, we show the evolution of the vertex divergence structures in the longitudinal sector for representative intermediate parameter sets between the limiting situations studied in Sec. IV C. These correspond to the case of $\alpha = 0^\circ$ [Fig. 2(a)] and $\alpha = 90^\circ$ [Fig. 2(b)] and are also reproduced for reference in Figs. 4(a) and 4(c), respectively. Note that, for the sake of clarity, we only show here the lowest [72] loop and parabola structures and their associated pseudodivergences.

We consider first the situation in which the variation of chemical potential is larger than the magnetic field, i.e., $0^\circ < \alpha < 45^\circ$, which we illustrate by showing, as an example, the case of $\alpha = 35^\circ$ in Fig. 4(d). Interestingly, for $U > 0$, in addition to the loop-structures and their associated pseudodivergences already discussed for $\alpha = 0^\circ$, a parabola structure appears at large values of βU . We can also observe that the pseudodivergence associated with this parabola at $U > 0$ is connected with the pseudodivergence emerging from the second parabola for $U < 0$.

In the reverse situation, where the magnetic field dominates over $\delta\mu$ (i.e., for $45^\circ < \alpha < 90^\circ$), in accordance with the mapping, the phase diagrams are geometrically identical (the projected weights differ, as is predicted by the mapping) to those for $\alpha' = 90^\circ - \alpha$, with $0^\circ < \alpha' < 45^\circ$, but for the flipping of the U and $-U$ sectors [see Fig. 4(f)].

Remarkably, for exactly $\alpha = 45^\circ$, where h equals $\delta\mu$, the loop structure touches its corresponding parabola at $U > 0$, while the same happens to the pair parabolas for $U < 0$. In both cases, at the point where the two structures touch, a perfectly horizontal (i.e., parallel to the r -axis) pseudodivergence line is emerging, as can be seen in Fig. 4(e).

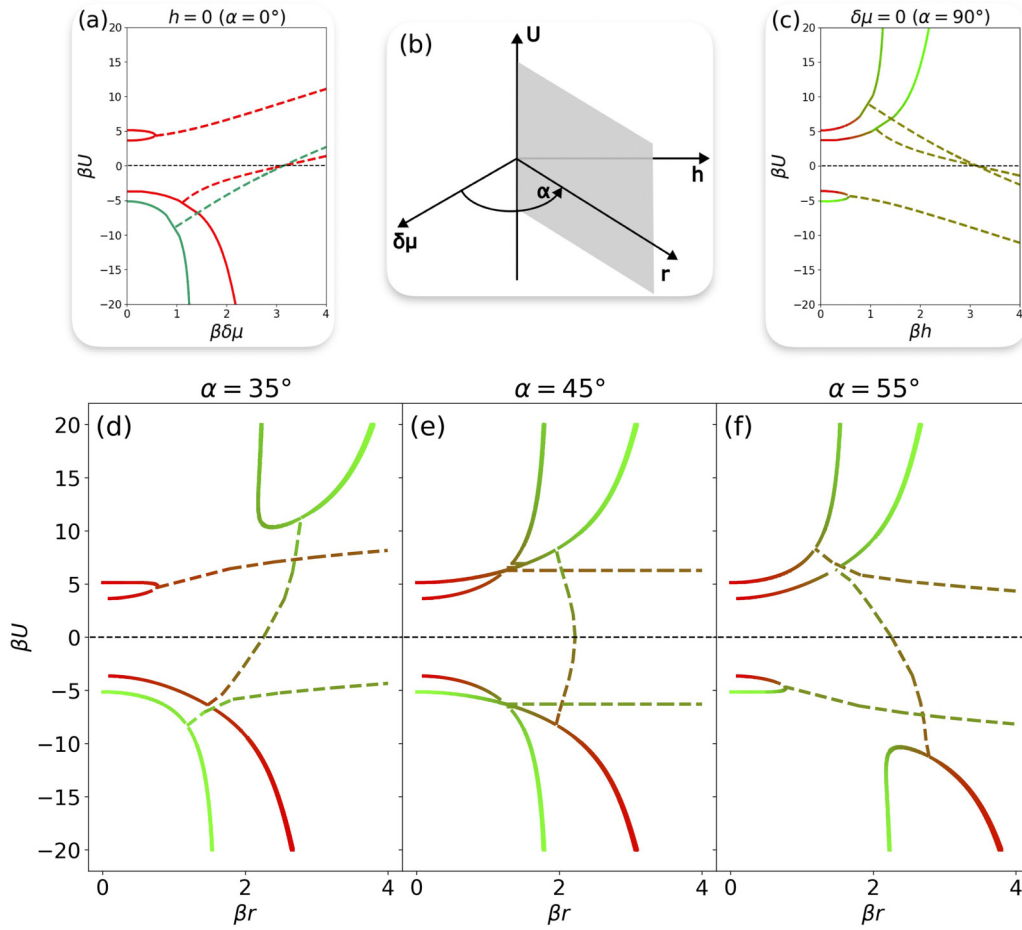


FIG. 4. (b) Sketch of the new coordinate system $\{U, r, \alpha\}$ introduced to systematically interpolate the illustration of the vertex (pseudo)divergences of the HA for arbitrary values of h and $\delta \mu$ between the limiting cases shown in Fig. 2, which correspond to $\alpha = 0^\circ$ and 90° . The corresponding (pseudo)divergences in the coupled longitudinal sector already shown in Fig. 2 are reproduced here, for reference, in (a) and (c). (d)–(f) Dimensionless phase space diagrams of the vertex (pseudo)divergences in the coupled longitudinal channel in the most general situation of finite magnetic field and arbitrary filling. Note that only the first divergence line structure is displayed for the different constant α planes chosen (see the text). The plotting conventions are as in Fig. 2.

Our results thus unveil the specific evolution of the vertex (pseudo)divergences between the two qualitatively different situations of $SU(2)_S$ and $SU(2)_P$ symmetries, and, in particular, how the loop-shaped divergence structures gets transformed in the parabola structures and vice versa. This also impacts the orientation of the pseudodivergence lines: One readily notes that those emerging from a parabola always cross the $U = 0$ axis at $r = \frac{v}{\sqrt{1 \pm 2 \cos \alpha \sin \alpha}}$, which is explicitly demonstrated in Eqs. (G8) and (G9), while the ones associated with the loops never cross the noninteracting axis. Evidently, the condition $\alpha = 45^\circ$ marks the change between these two behaviors, which is featured by the horizontal pseudodivergence lines.

Finally, in Fig. 5 we show for the same three exemplary cases as above (i.e., $\alpha = 35^\circ, 45^\circ, 55^\circ$) the vertex (pseudo)divergences in the transversal spin and in the pairing channel, restricting again the plot to the first structures for each channel. The (pseudo)divergence lines of the longitudinal channel shown in Fig. 6 are replotted in gray for reference.

All the divergence lines in these channels display a parabolic shape, consistent with the fact that, at particle-hole

symmetry, only symmetric divergences for both transversal channels exist. However, different from the longitudinal sector, the pseudodivergences associated with the transversal spin channel cross the $U = 0$ axis at $r = \frac{v}{\sqrt{(\cos \alpha)^2 - (\sin \alpha)^2}}$, i.e., only for $0^\circ \leq \alpha < 45^\circ$, while those of the pairing channel cross the $U = 0$ axis at $r = \frac{v}{\sqrt{(\sin \alpha)^2 - (\cos \alpha)^2}}$ and therefore only for $45^\circ < \alpha \leq 90^\circ$.

F. Mapping of the eigenvectors

Crucial information [29,32,35,39,54,56] on the possible physical effects associated with divergences is encoded in the frequency structure of the associated eigenvectors, and, especially, in their overall symmetry properties. While a detailed discussion of these properties is reported in Appendix A, which generalizes the corresponding particle-hole symmetric results of [29], here we illustrate some essential aspects of the eigenvector behavior by way of a pertinent example.

To this end, we consider the following two cases, directly related by the mapping, i.e., $\alpha = 35^\circ$ for $U > 0$ and $\alpha = 55^\circ$ for $U < 0$ (see the left panel of Fig. 6). The eigenvectors

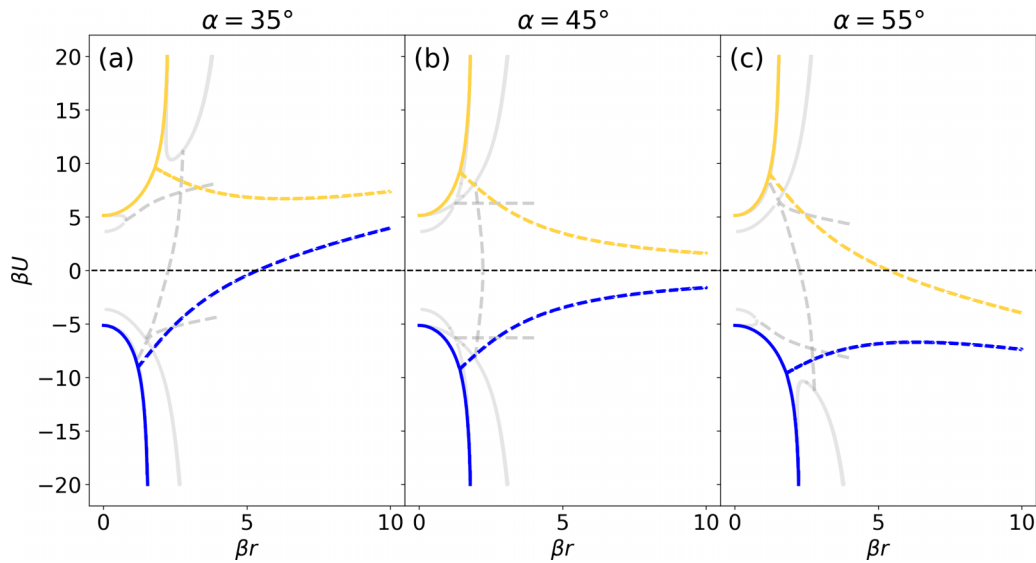


FIG. 5. Dimensionless phase space diagrams of the vertex (pseudo)divergences in the transversal spin channel (blue) and in the pairing channel (yellow) for the Hubbard atom. Note that only the first divergence line structure is displayed for different constant α -planes. The vertex (pseudo)divergences of the coupled longitudinal channel, already shown in Fig. 4, are reproduced here in gray for reference.

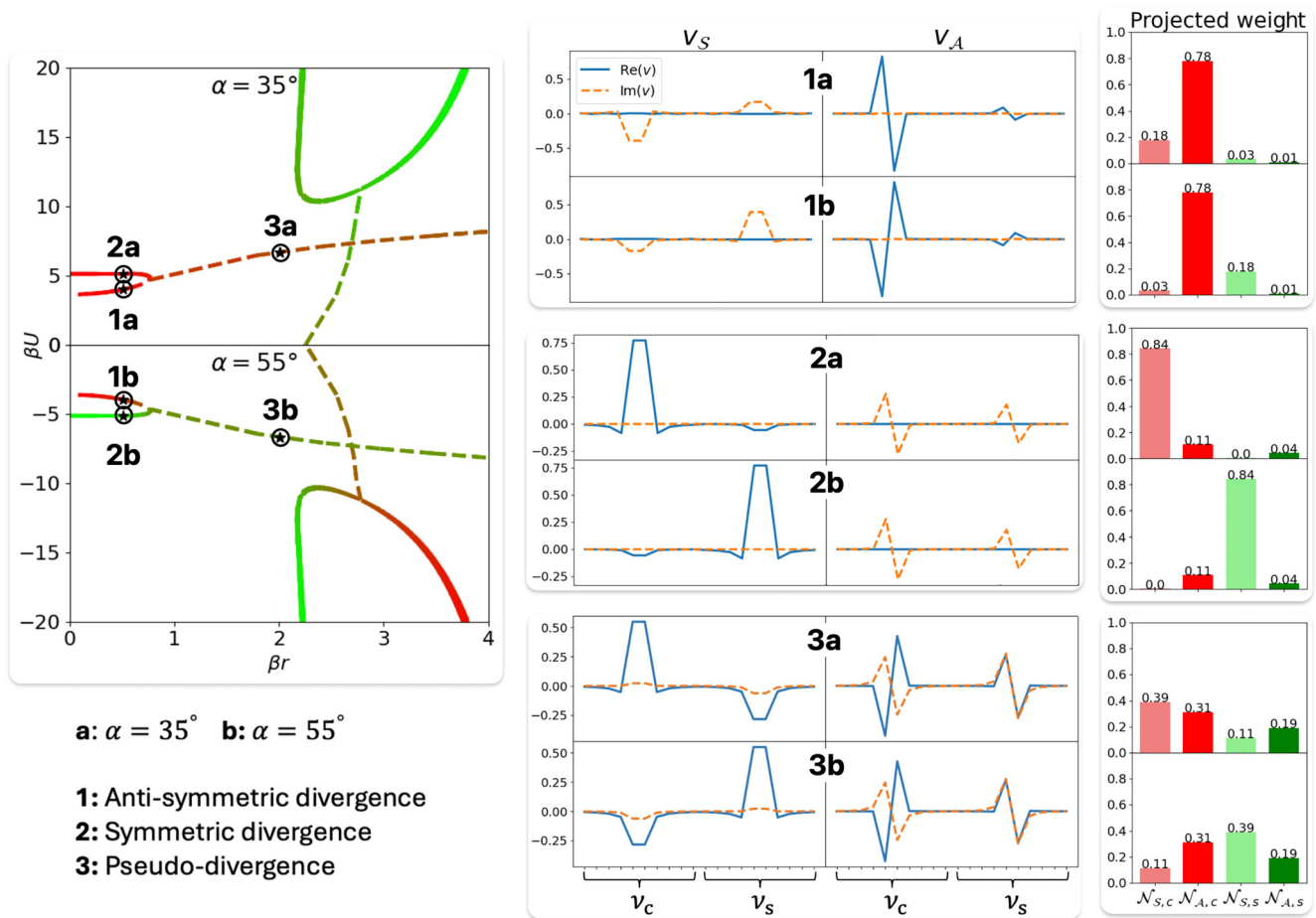


FIG. 6. Left: The phase space diagram of the vertex (pseudo)divergences in a longitudinal channel are shown for $\alpha = 35^\circ$ in the repulsive sector $U > 0$ and for $\alpha = 55^\circ$ in the attractive sector $U < 0$. These are the two cases that map into each other according to the mapping derived in Sec. III. The plotting conventions are as in Fig. 2. Middle: The eigenvectors that correspond to the (pseudo)divergence at specific points, which are marked by black stars. The eigenvectors are split into symmetric (v_S) and antisymmetric parts (v_A) to make the mapping more visible. Note that (a) always corresponds to $\alpha = 35^\circ$ while (b) corresponds to $\alpha = 55^\circ$. Right: The projected weights of the eigenvectors again split into symmetric and antisymmetric parts.

corresponding to the (pseudo)divergences of three selected parameter sets (marked by black stars in the left panel) are then shown in the central panel of the figure, where each eigenvector is split into its symmetric (v_S) and antisymmetric (v_A) part, while their projected weight in the charge and spin subspace (see Appendix E), calculated for the symmetric and antisymmetric part of each eigenvector, is shown in the rightmost panel.

According to the relations in Sec. III, the eigenvector marked by **1a** is mapped into **1b**, **2a** is mapped into **2b**, and **3a** into **3b**. When considering **1a** and **1b**, which are associated with an antisymmetric divergence of the vertex, we can observe the characteristic symmetry properties of the eigenvectors corresponding to a real eigenvalue in a κ -real matrix χ_L [see Eq. (A17)]. In particular, these eigenvectors split into a purely real antisymmetric part and an imaginary symmetric part. Analogously, **2a** and **2b**, associated with a symmetric divergence, display purely real symmetric/purely imaginary antisymmetric parts. On the other hand, **3a** and **3b** are one of the eigenvectors associated with a pseudodivergence, and hence with a pair of complex-conjugate eigenvalues. Therefore, the symmetric and antisymmetric parts of these eigenvectors are no longer purely real or imaginary. Note that only one of the eigenvectors of the pseudodivergence is shown since the other one can be reconstructed by Eq. (A17), and the projected weights of these two eigenvectors are the same.

Eventually, by comparing the **a** and **b** figures of each case, one can easily recognize the behavior predicted by the mapping relations derived in the previous section. The symmetric part of the eigenvector v_S changes from charge to spin subspace and vice versa, while the antisymmetric part v_A remains invariant under the mapping. This also reflects the relations of the corresponding weights, as it is readily seen when projecting the portion of the symmetric/antisymmetric part of the eigenvectors onto the charge or the spin subspace.

G. Finite bosonic transfer frequency

According to the current knowledge (cf. Ref. [32]), only irreducible vertex divergences occurring at $\omega = 0$ can be directly linked to the breakdown of the self-consistent perturbation theory for the many-electron problem. For this reason, the illustrative study of the (pseudo)divergences of the HA presented in this work is mostly focused on the $\omega = 0$ case.

Notwithstanding, for the sake of completeness, it is worthwhile to get a glimpse of some relevant modifications of the results presented so far, when considering vertex divergence structures at finite transfer frequency ($\omega \neq 0$). To this end, we will focus our discussion of the finite- ω case on the (pseudo)divergences occurring in the charge and spin sectors, when $SU(2)_S$ symmetry is preserved (i.e., $\delta\mu \neq 0$, $h = 0$). In this respect, our starting point will be represented by the findings of Ref. [22], where vertex divergences of the particle-hole symmetric HA ($\delta\mu = h = 0$) have been briefly analyzed for specific finite frequency values.

More precisely, the analytical expressions of Ref. [22] show that, for the ph-symmetric HA, vertex divergences occur at all βU values such that (i) $U = \pm \frac{2}{\sqrt{3}} \sqrt{v(v+\omega)}$ in the charge channel or (ii) $U = \pm 2 \sqrt{-v(v+\omega)}$ in the spin channel, where $v = \frac{(2n-1)\pi}{\beta}$ and $\omega = \frac{2m\pi}{\beta}$ are the

fermionic and the bosonic Matsubara frequencies, respectively. The eigenvectors associated with these divergences display an antisymmetric structure in the *shifted* frequency space Eq. (A12), i.e., they are proportional to $\delta_{v,v'} - \delta_{v,-v'-\omega}$.

Since the discriminant in the above relations (i) and (ii) must be positive, antisymmetric divergences in the spin channel can only occur for $\omega \neq 0$, when $v(v+\omega) < 0$. At the same time, for these frequency values no divergence can occur in the charge channel. However, the fulfillment of $v(v+\omega) < 0$ is not a sufficient condition for an antisymmetric divergence to occur, since antisymmetric eigenvectors require two distinct fermionic frequencies $v \neq -v-\omega$ for their construction. As a result, divergences in the spin channel only appear if $|m| > 1$, and a new antisymmetric divergence only appears at even m values.

Furthermore, vertex divergences associated with symmetric eigenvectors in the shifted frequency space can also be found [22], namely for all U values where

$$f_r = \frac{U \tan\left(\frac{\beta}{4}(\sqrt{4B_r^2 + \omega^2} + \omega)\right)}{\sqrt{4B_r^2 + \omega^2}} \pm 1 = 0 \quad (40)$$

is fulfilled, where the $+$ ($-$) sign is for the charge (spin) channel, and

$$B_c = \frac{U}{2} \sqrt{\frac{3e^{\beta U/2} - 1}{1 + e^{\beta U/2}}}, \quad (41)$$

$$B_s = -\frac{U}{2} \sqrt{\frac{3e^{-\beta U/2} - 1}{1 + e^{-\beta U/2}}}. \quad (42)$$

From Eq. (40) one finds [22] the occurrence of symmetric divergences in the charge channel for all values of ω if $U > 0$. However, we should note that the condition of Eq. (40) cannot be fulfilled if the corresponding eigenvector is maximal at a v value, for which $v(v+\omega) < 0$. Note that this is the same condition as for the antisymmetric divergences.

As for the symmetric divergences in the spin channel, contrary to what was reported in a side remark in Ref. [22], these can indeed occur at $U > 0$ for $m \geq 3$.

In summary, in the spin channel we find $\lfloor m/2 \rfloor$ antisymmetric divergences, while an explicit evaluation of Eq. (40) also yields $\lceil m/2 \rceil - 1$ symmetric divergences. At the same time, in the charge channel, infinitely many symmetric and antisymmetric divergences occur, under the condition that the corresponding eigenvectors do not have a maximum at frequencies where $v(v+\omega) < 0$.

The location of the first two symmetric and two antisymmetric divergences in the charge and spin channels is shown in Fig. 7 for different values of ω at ph-symmetry. The location of the divergences is symmetric in ω , i.e., it is the same for ω and $-\omega$.

For particle-hole symmetry, the action of the Shiba mapping at finite ω can be evidenced by noting that (i) all antisymmetric vertex divergences occur at the same absolute U values for positive and negative U , and (ii) f_c is transformed into $-f_s$ by changing U to $-U$. The latter condition implies that the symmetric vertex divergences for $U < 0$ can be obtained by just exchanging charge and spin channels in the discussion for $U > 0$. Hence, as a direct consequence of the Shiba mapping at finite frequency [see Eq. (33)], the findings

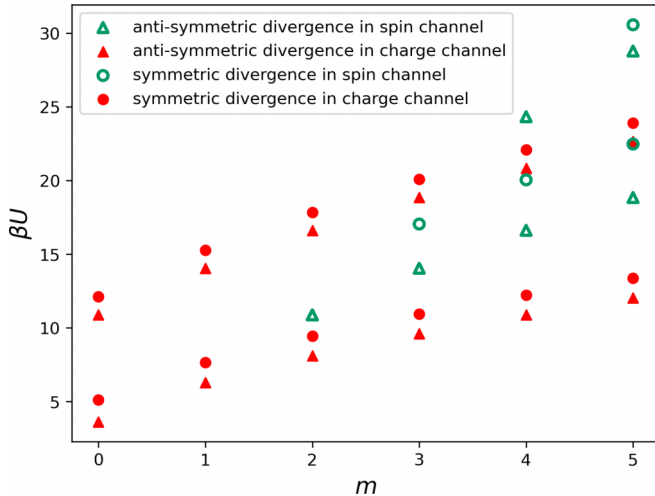


FIG. 7. Location of the first two symmetric and two antisymmetric vertex divergences in charge and spin channels at ph-symmetry for different $\omega = 2\pi m/\beta$ values.

of Ref. [29] for the vertex divergence of the static particle-hole case remain identically applicable also at $\omega \neq 0$.

At the same time, a remarkable difference from the $\omega = 0$ case is that negative real eigenvalues of the generalized charge/spin susceptibility at ph-symmetry can be found already at $U = 0$ [see Eq. (G1)], namely when the frequency condition $\nu(\nu + \omega) < 0$ is fulfilled. However, the role played by these negative eigenvalues in triggering additional divergences at $\omega \neq 0$ is quite different in the charge and in the spin channel. In fact, in the former one, consistently with the discussion above, the negative eigenvalues found at $U = 0$ never cross zero by increasing U . In the spin channel, instead, *all* negative eigenvalues found at $U = 0$ will cross zero by increasing U , except the ones that correspond to eigenvectors which either have their maximum at the central frequency $\nu^* = -\omega/2$ if m is odd or that are symmetric and have their maximum at $\nu = \omega/2 \pm \pi/\beta$ if m is even. Such crossings evidently trigger vertex divergences in the spin sector that were *not* present for $\omega = 0$.

Eventually, merging the description of the vertex divergences at finite ω for the ph-symmetric case [22] with the knowledge of the $\delta\mu$ -evolution of the vertex divergences at $\omega = 0$ (Sec. IV C), it becomes easy to intuitively outline their qualitative behavior as a function of a varying chemical potential. Specifically, by gradually increasing the absolute value of $\delta\mu$, we find that pairs of symmetric and antisymmetric vertex divergences get closer in parameter space, forming *loop*-structures in the phase diagram analogous to those shown in Fig. 2. In contrast, vertex divergences that do not have a partner at ph-symmetry, i.e., there exists no vertex divergence that has its maximum at the same frequency but has opposite symmetry, form a *parabola*-like structure in the phase space. Such divergences are, for example, the antisymmetric divergences in the spin channel for $m = 2, 4$ at the largest βU value shown in Fig. 7.

Hence, the overall evolution of the vertex (pseudo)divergence lines for $\omega \neq 0$ follows the intuitive expectation gained from the $\omega = 0$ case. This intuitive picture is quantitatively confirmed by direct calculations (not shown).

V. CONCLUSIONS

In this work, we have derived the explicit relations mapping the on-site two-particle generalized susceptibilities of bipartite lattice models with repulsive local interaction into those of corresponding models with attractive interaction and vice versa. The presented derivations, which exploit the Shiba transformation on the two-particle level (i) at arbitrary filling and/or in the presence of a finite magnetic field, as well as (ii) for finite transfer (bosonic) Matsubara frequency, extend the results of previous studies [29], which were restricted to the case of static correlation functions in the specific and less realistic situation of perfect particle-hole symmetry of the system.

Considering the increasing importance of the calculation and the manipulation of the two-particle quantities [20,21,23,28] for different cutting-edge algorithms [22,26,28] designed for treating strong correlations in many-electron systems, the explicit derivation of the mapping relations on the two-particle level might be useful in several contexts. For instance, it may allow us to reduce the computational effort of numerically heavy two-particle calculations in challenging parameter regimes and provide rigorous benchmark testbeds for computational schemes based on generalized on-site susceptibilities and vertex functions beyond the special case of particle-hole symmetry. Further, on a more fundamental level, our findings might represent a useful guide for an improved understanding of the information encoded in the correlation functions on the two-particle level.

In the latter respect, as a pertinent example for the applicability of the mapping relations, we have systematically analyzed the location and nature of the divergences of the irreducible vertex functions in the Hubbard atom with repulsive and attractive on-site interaction for arbitrary filling and finite magnetic field, overcoming the parameter restrictions of preceding studies [22,50]. The evident symmetries characterizing our dimensionless phase space diagrams for the divergences in the HA represent a direct consequence of the derived mapping relations. This consideration allows, in turn, for an easier comprehension of the intrinsic links existing between the various divergence structures in different parameter regimes of the HA.

Further, among the properties characterizing the evolution of the singularities in the different scattering channels as a function of filling and magnetic field, it may be worthwhile to stress here the appearance of the exceptional points (EPs) at which the vertex divergences (associated with a vanishing eigenvalue of the corresponding generalized susceptibility) transform into pseudodivergences (associated with a complex-conjugate eigenvalue pair with a zero real part). In fact, the relevance of these EPs has been discussed recently in the specific context of a possible topological protection [39] of the thermodynamic phase-separation instabilities emerging [35,54,56,73,74] in proximity to a Mott-Hubbard metal-to-insulator transitions of correlated lattice systems. At the same time, as demonstrated in Ref. [33], their occurrence is *not* limited to purely on-site four-point correlation functions. Eventually, the EPs might play, together with the pseudodivergences discussed in our work as well as with the pole structures [61] possibly appearing in the complex interaction plane [10], an important role in controlling the convergence properties of the self-consistent perturbation expansions for

the many-electron problem [22,31,32,75], *beyond* [33] the rather specific condition of perfect particle-hole symmetry mostly investigated so far.

A data set containing all numerical data and scripts for calculating and plotting these data is publicly available on the TU Wien Research Data repository [76].

ACKNOWLEDGMENTS

We want to thank Sabine Andergassen, Massimo Capone, Sergio Ciuchi, Lorenzo Crippa, Lorenzo Del Re, Dominik Fus, Marcel Gievers, Anna Kauch, Erik van Loon, Georg Rohringer, Stefan Rohshap, and Thomas Schäfer for insightful discussions. M.R. acknowledges financial support as a recipient of a DOC fellowship of the Austrian Academy of Sciences. G.S. acknowledges support from the Deutsche Forschungsgemeinschaft (DFG, German Research Foundation) through QUAST FOR 5249 (Project No. 449872909, project P5). This research was also funded by the Austrian Science Fund (FWF) via [doi:10.55776/I5487] (A.T.) and [doi:10.55776/I5868], Project No. P1 of the research unit FOR 5249 of the German research foundation (DFG) (H.E.). For open access purposes, the corresponding author (A.T.) has applied a CC BY public copyright license to any author accepted manuscript version arising from this submission. Calculations have been partly performed on the Vienna Scientific Cluster.

APPENDIX A: SYMMETRIES OF GENERALIZED SUSCEPTIBILITIES

In this Appendix, we study the properties of the local generalized susceptibilities for the symmetries considered in the main text, with a particular focus on $SU(2)_S$, $SU(2)_P$, and $SO(4)$ symmetry. For a detailed derivation of these symmetry properties and an in-depth discussion, the reader is referred to Ref. [38].

Doing a full particle-hole transformation ($c_\sigma \rightarrow c_\sigma^\dagger$, $c_\sigma^\dagger \rightarrow c_\sigma$) on the Hamiltonian in Eq. (12) gives

$$H(U, \delta\mu, h) \xrightarrow{\text{ph-trafo}} H(U, -\delta\mu, -h). \quad (\text{A1})$$

Therefore, the system is particle-hole symmetric (i.e., the Hamiltonian is invariant under the particle-hole transformation) if $\delta\mu = h = 0$, which corresponds to $SO(4)$ symmetry.

Further, applying a full particle-hole transformation in the definitions of Eqs. (1) and (2) and then using crossing symmetry and complex conjugation [Eqs. (A6) and (A7)] lead to

$$\chi \xrightarrow{\text{ph-trafo}} \chi^*, \quad (\text{A2})$$

and a sign change in the magnetic field just flips all spins of the generalized susceptibility ($\sigma \rightarrow -\sigma$, $\forall \sigma$).

We find the following relations for the different channels: In the coupled longitudinal channel

$$\begin{aligned} \chi_L &\xrightarrow{\delta\mu, h \leftrightarrow -\delta\mu, -h} \chi_L^*, \\ \chi_L &\xrightarrow{h \leftrightarrow -h} M \chi_L M, \\ \chi_L &\xrightarrow{\delta\mu \leftrightarrow -\delta\mu} M \chi_L^* M, \end{aligned} \quad (\text{A3})$$

where $M = \begin{pmatrix} 1 & 0 \\ 0 & -1 \end{pmatrix}$, and for the transversal spin and the pairing channel we find

$$\begin{aligned} \chi_{S_x} &\xrightarrow{\delta\mu, h \leftrightarrow -\delta\mu, -h} \chi_{S_x}^*, \\ \chi_{S_x} &\xrightarrow{h \leftrightarrow -h} \chi_{S_x}, \end{aligned} \quad (\text{A4})$$

$$\begin{aligned} \chi_{S_x} &\xrightarrow{\delta\mu \leftrightarrow -\delta\mu} \chi_{S_x}^*, \\ \chi_{\text{pair}} &\xrightarrow{\delta\mu, h \leftrightarrow -\delta\mu, -h} \chi_{\text{pair}}^*, \\ \chi_{\text{pair}} &\xrightarrow{h \leftrightarrow -h} \chi_{\text{pair}}^*, \\ \chi_{\text{pair}} &\xrightarrow{\delta\mu \leftrightarrow -\delta\mu} \chi_{\text{pair}}. \end{aligned} \quad (\text{A5})$$

Since the transformations in Eqs. (A3)–(A5) change neither the eigenvalues nor the projected weights [see Eq. (E2)] of the generalized susceptibility matrices, we confirm that the whole phase space can be generated by mapping the calculated quantities from the sub-region where $\delta\mu > 0$ and $h > 0$. This corresponds to the interval $\alpha \in [0^\circ, 90^\circ]$ in the cylinder coordinates of Eq. (38).

In Eqs. (A6)–(A10) the properties of the generalized susceptibilities under the specific symmetry relations are explicitly written following Ref. [38].

Crossing symmetry and complex conjugation are fundamental “symmetries,” i.e., they are always present, $H \in \mathbb{R}$ refers to the Hamiltonian being a real function of c and c^\dagger , and $SU(2)_S/SU(2)_P$ means symmetric with respect to spin/pseudospin,

$$\begin{aligned} \text{Crossing symmetry: } \chi_{\sigma\sigma', \text{ph}}^{v, v', \omega} &= \chi_{\sigma'\sigma, \text{ph}}^{\omega+v', \omega+v, -\omega}, \\ \chi_{\sigma\sigma', \text{ph}}^{v, v', \omega} &= \chi_{\sigma'\sigma, \text{ph}}^{\omega+v', \omega+v, -\omega}, \\ \chi_{\sigma\sigma', \text{pp}}^{v, v', \omega} &= \chi_{\sigma'\sigma, \text{pp}}^{\omega-v, \omega-v', \omega}, \end{aligned} \quad (\text{A6})$$

$$\begin{aligned} \text{Complex conjugation: } \chi_{\sigma\sigma', \text{ph}}^{v, v', \omega} &= (\chi_{\sigma'\sigma, \text{ph}}^{-v', -v, -\omega})^*, \\ \chi_{\sigma\sigma', \text{ph}}^{v, v', \omega} &= (\chi_{\sigma'\sigma, \text{ph}}^{-v', -v, -\omega})^*, \\ \chi_{\sigma\sigma', \text{pp}}^{v, v', \omega} &= (\chi_{\sigma'\sigma, \text{pp}}^{-v', -v, -\omega})^*, \end{aligned} \quad (\text{A7})$$

$$\begin{aligned} \hat{H} \in \mathbb{R}: \chi_{\sigma\sigma', \text{ph}}^{v, v', \omega} &= \chi_{\sigma'\sigma, \text{ph}}^{v', v, \omega}, \\ \chi_{\sigma\sigma', \text{ph}}^{v, v', \omega} &= \chi_{\sigma'\sigma, \text{ph}}^{v', v, \omega}, \\ \chi_{\sigma\sigma', \text{pp}}^{v, v', \omega} &= \chi_{\sigma'\sigma, \text{pp}}^{v', v, \omega}, \end{aligned} \quad (\text{A8})$$

$$\begin{aligned} \text{SU}(2)_S \text{ symmetry: } \chi_{\sigma\sigma', \text{ph}}^{v, v', \omega} &= \chi_{-\sigma-\sigma', \text{ph}}^{v, v', \omega}, \\ \chi_{\sigma\sigma', \text{ph}}^{v, v', \omega} &= \chi_{-\sigma-\sigma', \text{ph}}^{v, v', \omega}, \\ \chi_{\sigma\sigma', \text{pp}}^{v, v', \omega} &= \chi_{-\sigma-\sigma', \text{pp}}^{v, v', \omega}, \end{aligned} \quad (\text{A9})$$

$$\begin{aligned} \text{SU}(2)_P \text{ symmetry: } \chi_{\sigma\sigma', \text{ph}}^{v, v', \omega} &= (\chi_{-\sigma-\sigma', \text{ph}}^{v, v', \omega})^*, \\ \chi_{\sigma\sigma', \text{ph}}^{v, v', \omega} &= (\chi_{-\sigma-\sigma', \text{ph}}^{v, v', \omega})^*, \\ \chi_{\sigma\sigma', \text{pp}}^{v, v', \omega} &= (\chi_{-\sigma-\sigma', \text{pp}}^{v, v', \omega})^*. \end{aligned} \quad (\text{A10})$$

From Eqs. (A6)–(A10), the relations written in Table I of the main text can be derived.

In the following, we introduce the class of centro-Hermitian matrices C which fulfill

$$JC^*J = C \quad \text{with } J = \begin{pmatrix} & & & 1 \\ & & \ddots & \\ & & & \\ 1 & & & \end{pmatrix}. \quad (\text{A11})$$

Centro-Hermitian matrices have eigenvalues that are either real or come in complex-conjugate pairs [40].

By using the symmetry Eqs. (A6)–(A8), we find that all generalized susceptibilities are centro-Hermitian for $\omega = 0$. Note that for $\chi_{\sigma\sigma',\text{ph}}^{\omega=0}$ the centro-Hermitian property is fundamental, since only complex conjugation and crossing symmetry (which are always present) are needed, whereas for $\chi_{\sigma\sigma',\text{ph/pp}}^{\omega=0}$ also $H \in \mathbb{R}$ is required (which could be violated in principle). Without this restriction $\chi_{\sigma\sigma',\text{ph/pp}}^{\omega=0}$, are per-Hermitian matrices [39].

Moreover, $\chi_{\sigma\sigma',\text{ph}}$ can be considered as a centro-Hermitian matrix for finite ω when shifting the fermionic Matsubara frequencies by $\nu^{(\prime)} \rightarrow \nu^{(\prime)} + \lfloor m/2 \rfloor 2\pi/\beta$ with $\omega = 2\pi m/\beta$ [$\lfloor x \rfloor$ refers to floor(x)]. This leads to

$$\begin{aligned} \chi_{\sigma\sigma',\text{ph}}^{\nu,\nu',\omega} &= (\chi_{\sigma\sigma',\text{ph}}^{-\nu-\omega, -\nu'-\omega, \omega})^* \\ &\downarrow \text{frequency shift} \\ \chi_{\sigma\sigma',\text{ph}}^{\nu-\lfloor \omega/2 \rfloor, \nu'-\lfloor \omega/2 \rfloor, \omega} &= (\chi_{\sigma\sigma',\text{ph}}^{-\nu-\lfloor \omega/2 \rfloor, -\nu'-\lfloor \omega/2 \rfloor, \omega})^*, \end{aligned} \quad (\text{A12})$$

where $\lfloor \omega/2 \rfloor$ is a short-hand notation for $\lfloor m/2 \rfloor 2\pi/\beta$ such that $\nu - \omega/2$ is still a fermionic Matsubara frequency. Thus, for any bosonic frequency ω , $\chi_{\sigma\sigma',\text{ph}}$ is a centro-Hermitian matrix in the frequency shifted space.

Moreover, we introduce the class of κ -real matrices [41], which also have only real or complex-conjugate pairs as eigenvalues. The generalized susceptibility of the coupled longitudinal channel χ_L is a κ -real matrix that fulfills the relation

$$\Pi K^* \Pi = K \quad \text{with } \Pi = \begin{pmatrix} J & 0 \\ 0 & J \end{pmatrix}. \quad (\text{A13})$$

Further, all considered channels are symmetric matrices if $H \in \mathbb{R}$ and can be diagonalized by a complex orthogonal transformation if there is no exceptional point. The corresponding inner product of the orthogonal Euclidean quasinorm is defined as

$$\langle u, v \rangle := u^T \cdot v = \sum_i^n u_i v_i \quad (\text{A14})$$

and

$$\|u\|_T^2 := u^T \cdot u. \quad (\text{A15})$$

Eigenvectors of symmetric and centro-Hermitian matrices that are normalized with respect to Eq. (A15) have the following properties [39]:

$$\begin{aligned} \text{if } \lambda_\alpha \in \mathbb{R} \text{ (and not degenerate): } v_\alpha &= \pm J v_\alpha^*, \\ \text{if } \lambda_\alpha \in \mathbb{C} : \exists v_{\alpha'} &= J v_\alpha^*, \end{aligned} \quad (\text{A16})$$

where the relation for real eigenvalues leads to the fact that their eigenvectors have a symmetric/antisymmetric real part with an antisymmetric/symmetric imaginary part (with respect to the shifted Matsubara frequency space $\nu^{(\prime)} \rightarrow \nu^{(\prime)} + \lfloor m/2 \rfloor 2\pi/\beta$).

For the symmetric κ -real matrix χ_L , we can make a similar argument to that in Ref. [39] to obtain

$$\begin{aligned} \text{if } \lambda_\alpha \in \mathbb{R} \text{ (and not degenerate): } v_\alpha &= \pm \Pi v_\alpha^*, \\ \text{if } \lambda_\alpha \in \mathbb{C} : \exists v_{\alpha'} &= \Pi v_\alpha^*, \end{aligned} \quad (\text{A17})$$

where the relation for real eigenvalues leads to the fact that their eigenvectors have a symmetric/antisymmetric real part with an antisymmetric/symmetric imaginary part in the charge and spin subspaces, respectively (with respect to the shifted Matsubara frequency space).

APPENDIX B: BSE OF THE TRANSVERSAL CHANNEL

In general, χ_{S_x} and χ_{pair} do not represent decoupled channels in the BSE. Even though $\chi_{S_x} = \chi_{S_y}$, they still couple to each other for $\langle S_z \rangle \neq 0$ [19]. The same considerations apply to the real and imaginary part of the pairing field Δ , which are given by $S_{p,x}$ and $S_{p,y}$, and couple for $\langle S_{p,z} \rangle \neq 0$. Therefore, the S_x /pairing channel generally (for arbitrary ω) only decouples within the transversal subspace when $SU(2)_{S/P}$ symmetry is fulfilled. This can be shown from the symmetry relations in Appendix A and the expressions of the coupled channels in Eqs. (B1) and (B2). This is an example of how the mapping “preserves” the decoupling of the channels regarding the BSE. Instead the transverse components $\chi_{\sigma\sigma'}$ and $\chi_{\sigma\sigma',\text{pp}}$ remain independent in the BSE. Hence, for the respective generalized susceptibility of the coupled BSE, we have to consider the transversal ph-channel (or $\chi_{\sigma\sigma'}$ directly)

$$\chi_T = \begin{pmatrix} \chi_{\uparrow\downarrow} + \chi_{\downarrow\uparrow} & \chi_{\uparrow\downarrow} - \chi_{\downarrow\uparrow} \\ \chi_{\uparrow\downarrow} - \chi_{\downarrow\uparrow} & \chi_{\uparrow\downarrow} + \chi_{\downarrow\uparrow} \end{pmatrix} \quad (\text{B1})$$

instead of the spin channel, and the transversal pp-channel (or $\chi_{\sigma\sigma',\text{pp}}$ directly)

$$\chi_{T,\text{pp}} = \begin{pmatrix} -\chi_{\uparrow\downarrow,\text{pp}} - \chi_{\downarrow\uparrow,\text{pp}}^* & -\chi_{\uparrow\downarrow,\text{pp}} + \chi_{\downarrow\uparrow,\text{pp}}^* \\ -\chi_{\uparrow\downarrow} + \chi_{\downarrow\uparrow}^* & -\chi_{\uparrow\downarrow,\text{pp}} - \chi_{\downarrow\uparrow,\text{pp}}^* \end{pmatrix} \quad (\text{B2})$$

instead of the pairing channel. If the Hamiltonian is a real function of c and c^\dagger , then $\chi_{\uparrow\downarrow}^{\nu,\nu',\omega} = \chi_{\downarrow\uparrow}^{\omega+\nu, \omega+\nu', -\omega}$ and $\chi_{\uparrow\downarrow,\text{pp}}^{\nu,\nu',\omega} = (\chi_{\downarrow\uparrow,\text{pp}}^{\nu-\omega, \nu'-\omega, \omega})^*$ (see Appendix A), and both the BSE of the pairing channel and the transversal spin channel decouple for $\omega = 0$. Hence, to investigate the divergences of the two-particle irreducible vertices for $\omega = 0$, χ_{S_x} and χ_{pair} can be used for the scope of this paper, as is done in Sec. IV.

APPENDIX C: CALCULATIONS FOR THE SHIBA MAPPING OF THE GENERALIZED SUSCEPTIBILITIES

In this Appendix, we derive the action of the Shiba transformation applied to the local generalized susceptibilities. The results of this transformation are shown in Sec. III. For the derivation we start by showing how the orthogonal

transformation

$$Q = \frac{1}{\sqrt{2}} \begin{pmatrix} \mathbb{1} & -J \\ \mathbb{1} & J \end{pmatrix} \quad (C1)$$

separates the symmetric and antisymmetric parts of a centro-Hermitian matrix. Every centro-Hermitian matrix χ_{CH} can be represented by the sum of a centrosymmetric real matrix χ' ($J\chi'J = \chi'$) and a skew-centro-symmetric imaginary matrix χ'' ($J\chi''J = -\chi''$).

For even dimensions, a centro-Hermitian matrix can be represented by

$$\chi_{\text{CH}} = \chi' + i\chi'' \quad \text{with} \quad \chi' = \begin{pmatrix} A' & JB'J \\ B' & JA'J \end{pmatrix}, \quad (C2)$$

$$\chi'' = \begin{pmatrix} A'' & -JB''J \\ B'' & -JA''J \end{pmatrix},$$

where $\chi^{(\prime)}$, $A^{(\prime)}$, and $B^{(\prime)}$ are real square matrices.

The transformation Q acts on (skew-)centro-symmetric matrices as follows:

$$Q\chi'Q^T = \begin{pmatrix} A' - JB' & 0 \\ 0 & A' + JB' \end{pmatrix} \quad (C3)$$

and

$$Q\chi''Q^T = \begin{pmatrix} 0 & A'' - JB'' \\ A'' + JB'' & 0 \end{pmatrix}. \quad (C4)$$

$A' - JB'$ and $A'' + JB''$ are referred to as antisymmetric blocks, and $A' + JB'$ and $A'' - JB''$ are termed symmetric blocks. To understand why, we let χ' and χ'' act on a generic vector v that is decomposed into symmetric and antisymmetric parts:

$$\chi'v = \begin{pmatrix} A' & JB'J \\ B' & JA'J \end{pmatrix} \left[\begin{pmatrix} v_S \\ Jv_S \end{pmatrix} + \begin{pmatrix} v_A \\ -Jv_A \end{pmatrix} \right]$$

$$= \begin{pmatrix} (A' + JB')v_S + (A' - JB')v_A \\ (A' + JB')v_S + (A' - JB')v_A \end{pmatrix} \quad (C5)$$

and

$$\chi''v = \begin{pmatrix} A'' & -JB''J \\ B'' & -JA''J \end{pmatrix} \left[\begin{pmatrix} v_S \\ Jv_S \end{pmatrix} + \begin{pmatrix} v_A \\ -Jv_A \end{pmatrix} \right]$$

$$= \begin{pmatrix} (A'' - JB'')v_S + (A'' + JB'')v_A \\ (A'' - JB'')v_S + (A'' + JB'')v_A \end{pmatrix}. \quad (C6)$$

As can be seen, $A' - JB'$ and $A'' + JB''$ couple to the antisymmetric part of the vector, and $A' + JB'$ and $A'' - JB''$ couple to the symmetric part of the vector.

Therefore, we identify the blocks in Eq. (31) by

$$\begin{aligned} \chi'_A &= A' - JB', \\ \chi'_S &= A' + JB', \\ \chi''_A &= A'' + JB'', \\ \chi''_S &= A'' - JB''. \end{aligned} \quad (C7)$$

As described in Appendix A, the generalized susceptibility $\chi_{\sigma\sigma',\text{ph}}$ is still a centro-Hermitian matrix for $\omega \neq 0$ if we

consider the shifted space $v^{(\prime)} \rightarrow v^{(\prime)} + \lfloor m/2 \rfloor 2\pi/\beta$ with $\omega = 2m\pi/\beta$. As already mentioned in the main text, the derivation for even m is completely analogous to the $\omega = 0$ case if the shifted space is considered.

However, for odd m slight adaptations are needed since the matrix acquires an odd frequency structure with a new central frequency $\nu^* = -\omega/2$. In other words, if we consider a finite frequency box (e.g., in numerical calculations), the frequency shift leads to a $(2N) \times (2N)$ matrix for even m and to a $(2N + 1) \times (2N + 1)$ matrix for odd m .

A centro-Hermitian matrix of odd dimension can be depicted by

$$\chi_{\text{CH}} = \chi' + i\chi'' \quad \text{with} \quad \chi' = \begin{pmatrix} A' & a' & JB'J \\ b' & c & b'J \\ B' & Ja' & JA'J \end{pmatrix},$$

$$\chi'' = \begin{pmatrix} A'' & a'' & -JB''J \\ b'' & 0 & -b''J \\ B'' & -Ja'' & -JA''J \end{pmatrix}, \quad (C8)$$

where $A, B \in \mathbb{R}^{N \times N}$, $a \in \mathbb{R}^{N \times 1}$, $b \in \mathbb{R}^{1 \times N}$, and $c \in \mathbb{R}$. With

$$Q = \frac{1}{\sqrt{2}} \begin{pmatrix} \mathbb{1} & 0 & -J \\ 0 & \sqrt{2} & 0 \\ \mathbb{1} & 0 & J \end{pmatrix} \quad (C9)$$

we can apply the transformation $Q\chi_{\text{CH}}Q^T$, in the same way as for the even-dimensional case to identify the symmetric and antisymmetric blocks of the matrix in Eq. (31):

$$\begin{aligned} \chi'_{A'} &= A' - JB', \\ \chi'_{S'} &= \begin{pmatrix} c & \sqrt{2}b' \\ \sqrt{2}a' & A' + JB' \end{pmatrix}, \\ \chi''_{A''} &= \begin{pmatrix} \sqrt{2}b'' \\ A'' + JB'' \end{pmatrix}, \\ \chi''_{S''} &= (\sqrt{2}a'', \quad A'' - JB''). \end{aligned} \quad (C10)$$

Now we can start with the derivation of the mapping of the generalized susceptibilities by writing the action of the Shiba transformation in Eq. (28) as matrix products in the frequency shifted space:

$$\begin{aligned} \chi_{\uparrow\uparrow,U} &= \chi_{\uparrow\uparrow,-U}, \quad \chi_{\downarrow\downarrow,U} = J\chi_{\downarrow\downarrow,-U}J, \\ \chi_{\uparrow\downarrow,U} &= -\chi_{\uparrow\downarrow,-U}J, \quad \text{and} \quad \chi_{\downarrow\uparrow,U} = -J\chi_{\downarrow\uparrow,-U}. \end{aligned} \quad (C11)$$

With these building blocks, we can construct the coupled longitudinal matrix

$$\chi_{\text{L}} = \begin{pmatrix} \chi_{\text{c}} & \chi_{\text{cs}} \\ \chi_{\text{sc}} & \chi_{\text{s}} \end{pmatrix} \quad (C12)$$

and then apply the transformation

$$Q = \begin{pmatrix} Q & 0 \\ 0 & Q \end{pmatrix} \quad (\text{C13})$$

to it.

With simple matrix multiplication, we obtain

$$\begin{aligned} Q\chi_{L,U}Q^T &= \begin{pmatrix} Q\chi_{c,U}Q^T & Q\chi_{cs,U}Q^T \\ Q\chi_{sc,U}Q^T & Q\chi_{s,U}Q^T \end{pmatrix} \\ &= \begin{pmatrix} \chi'_{c,U,A} & i\chi''_{c,U,S} & \chi'_{cs,U,A} & i\chi''_{cs,U,S} \\ i\chi''_{c,U,A} & \chi'_{c,U,S} & i\chi''_{cs,U,A} & \chi'_{cs,U,S} \\ \chi'_{sc,U,A} & i\chi''_{sc,U,S} & \chi'_{s,U,A} & i\chi''_{s,U,S} \\ i\chi''_{sc,U,A} & \chi'_{sc,U,S} & i\chi''_{s,U,A} & \chi'_{s,U,S} \end{pmatrix} \\ &= \begin{pmatrix} \chi'_{c,U,A} & i\chi''_{cs,U,S} & \chi'_{cs,U,A} & i\chi''_{c,U,S} \\ i\chi''_{sc,U,A} & \chi'_{s,U,S} & i\chi''_{s,U,A} & \chi'_{sc,U,S} \\ \chi'_{sc,U,A} & i\chi''_{s,U,S} & \chi'_{s,U,A} & i\chi''_{sc,U,S} \\ i\chi''_{c,U,A} & \chi'_{cs,U,S} & i\chi''_{cs,U,A} & \chi'_{c,U,S} \end{pmatrix} \\ &= TQ\chi_{L,U}Q^T T, \end{aligned} \quad (\text{C14})$$

where an appropriate Q matrix has to be used depending on whether the generalized susceptibility is an even or an odd matrix. From Eq. (C14) and the fact that Q is an orthogonal transformation, Eq. (33) in the main text is obtained.

In Eq. (C14) one can see that after the Q transformation, $\chi_{L,U}$ and $\chi_{L,-U}$ only differ by a permutation of the different submatrices. This reshuffling is done by the matrix T in Eq. (32), which needs to be adapted to Eq. (C15) for the odd-dimensional case

$$T = \begin{pmatrix} \mathbb{1} & 0 & 0 & 0 & 0 & 0 \\ 0 & 0 & 0 & 0 & 1 & 0 \\ 0 & 0 & 0 & 0 & 0 & \mathbb{1} \\ 0 & 0 & 0 & \mathbb{1} & 0 & 0 \\ 0 & 1 & 0 & 0 & 0 & 0 \\ 0 & 0 & \mathbb{1} & 0 & 0 & 0 \end{pmatrix}. \quad (\text{C15})$$

We find that (i) a symmetric/antisymmetric block of $\chi_{L,U}$ always maps to a symmetric/antisymmetric block of $\chi_{L,-U}$, and (ii) all $\chi'_{\mathcal{A}}$ blocks are invariant under the mapping. All other blocks get redistributed according to Eq. (C14), which is summarized in Eqs. (34) and (35) in the main text [77]. Note that for χ_L the subscript \mathcal{A}/\mathcal{S} refers to the coupling of the respective anti-/symmetric components in the charge and spin subspace of a generic vector v . For the even-dimensional case,

$$v = \begin{pmatrix} v_{c,S} \\ Jv_{c,S} \\ v_{s,S} \\ Jv_{s,S} \end{pmatrix} + \begin{pmatrix} v_{c,A} \\ -Jv_{c,A} \\ v_{s,A} \\ -Jv_{s,A} \end{pmatrix} \quad (\text{C16})$$

and for the odd-dimensional case,

$$v = \begin{pmatrix} v_{c,S} \\ m_c \\ Jv_{c,S} \\ v_{s,S} \\ m_s \\ Jv_{s,S} \end{pmatrix} + \begin{pmatrix} v_{c,A} \\ 0 \\ -Jv_{c,A} \\ v_{s,A} \\ 0 \\ -Jv_{s,A} \end{pmatrix}. \quad (\text{C17})$$

Eventually, we consider the action of the Shiba transformation $S = Q^T T Q$, which is orthogonal and symmetric, on the eigenvectors and eigenvalues of χ_L .

Since S is an orthogonal transformation, $\chi_{L,U}$ and $\chi_{L,-U}$ have the same eigenvalues. Further, if v is an eigenvector of $\chi_{L,U}$, then Sv is an eigenvector of $\chi_{L,-U}$ with the same eigenvalue. Transforming the eigenvector v , we find

$$\begin{aligned} Sv &= S \left[\begin{pmatrix} v_{c,S} \\ Jv_{c,S} \\ v_{s,S} \\ Jv_{s,S} \end{pmatrix} + \begin{pmatrix} v_{c,A} \\ -Jv_{c,A} \\ v_{s,A} \\ -Jv_{s,A} \end{pmatrix} \right] \\ &= \begin{pmatrix} v_{c,S} \\ Jv_{c,S} \\ v_{c,S} \\ Jv_{c,S} \end{pmatrix} + \begin{pmatrix} v_{c,A} \\ -Jv_{c,A} \\ v_{s,A} \\ -Jv_{s,A} \end{pmatrix} \end{aligned} \quad (\text{C18})$$

for the even-dimensional case, and

$$\begin{aligned} Sv &= S \left[\begin{pmatrix} v_{c,S} \\ m_c \\ Jv_{c,S} \\ v_{s,S} \\ m_s \\ Jv_{s,S} \end{pmatrix} + \begin{pmatrix} v_{c,A} \\ 0 \\ -Jv_{c,A} \\ v_{s,A} \\ 0 \\ -Jv_{s,A} \end{pmatrix} \right] \\ &= \begin{pmatrix} v_{c,S} \\ m_s \\ Jv_{c,S} \\ v_{c,S} \\ m_c \\ Jv_{c,S} \end{pmatrix} + \begin{pmatrix} v_{c,A} \\ 0 \\ -Jv_{c,A} \\ v_{s,A} \\ 0 \\ -Jv_{s,A} \end{pmatrix} \end{aligned} \quad (\text{C19})$$

for the odd-dimensional case. Evidently, the symmetric part of the eigenvector changes the subspace between charge and spin, while the antisymmetric part of the eigenvector is invariant under the transformation.

To obtain the Shiba transformation for the generalized susceptibility in the transverse spin channel χ_{S_x} , we apply the Shiba transformation on Eq. (2) and get

$$\begin{aligned} \chi_{\uparrow\downarrow,U}^{v,v',\omega} &= -\chi_{\uparrow\downarrow,-U}^{v,v',-\nu-v'-\omega} = -\chi_{\uparrow\downarrow,pp,-U}^{v,v',-\omega}, \\ \chi_{\uparrow\downarrow,U}^{v,v',\omega} &= -\chi_{\uparrow\downarrow,-U}^{-\nu,-v',\nu+v'+\omega} = -\chi_{\uparrow\downarrow,pp,-U}^{-\nu,-v',\omega} = -(\chi_{\uparrow\downarrow,pp,-U}^{v,v',-\omega})^*, \end{aligned} \quad (\text{C20})$$

where we use the fact that shifting $\omega \rightarrow \omega - \nu - v'$ is changing the ph-convention to the pp-convention, and in the second line we applied the property for complex conjugation Eq. (A7).

Together with the definition of $\chi_{S_x}^{v,v',\omega}$ and $\chi_{\text{pair}}^{v,v',\omega}$ in (8) and (9), we get

$$\chi_{S_x,U}^{v,v',\omega} = \chi_{\text{pair},-U}^{v,v',-\omega}, \quad (\text{C21})$$

which is, in our notation, equivalent to Eq. (36) in the main text.

APPENDIX D: ANALYTICAL EXPRESSION FOR THE GENERALIZED SUSCEPTIBILITY IN THE HUBBARD ATOM

Following Ref. [44], the one-particle Green's function and the connected two-particle Green's functions for the HA in notation for different spin combinations are as follows:

$$G_{1,\sigma}(v) = \frac{1 - n_{-\sigma}}{iv + \mu + \sigma h} + \frac{n_{-\sigma}}{iv + \mu + \sigma h - U}, \quad (\text{D1})$$

$$G_{2,\uparrow\uparrow}^{\text{con}}(v, v', \omega) = \frac{\beta U^2 n_{\downarrow} (\delta_{\omega 0} - \delta_{vv'})}{(iv + i\omega + \mu + h)(iv + i\omega + \mu + h - U)(iv' + \mu + h)(iv' + \mu + h - U)}, \quad (\text{D2})$$

$$\begin{aligned} G_{2,\uparrow\downarrow}^{\text{con}}(v, v', \omega) &= \frac{n_{\uparrow} + n_{\downarrow} - 1}{iv + iv' + i\omega + 2\mu - U} \left(\frac{1}{iv + i\omega + \mu + h - U} + \frac{1}{iv' + \mu - h - U} \right) \left(\frac{1}{iv' + i\omega + \mu - h - U} + \frac{1}{iv + \mu + h - U} \right) \\ &+ \frac{n_{\uparrow} - n_{\downarrow}}{iv' - iv - 2h} \left(\frac{1}{iv' + \mu - h} - \frac{1}{iv + \mu + h - U} \right) \left(\frac{1}{iv' + i\omega + \mu - h} - \frac{1}{iv + i\omega + \mu + h - U} \right) \\ &+ \frac{\beta U^2 \delta_{\omega 0} (e^{(2\mu-U)\beta} - e^{2\mu\beta})}{(1 + e^{(\mu+h)\beta} + e^{(\mu-h)\beta} + e^{(2\mu-U)\beta})^2} \frac{1}{(iv + \mu + h)(iv + \mu + h - U)(iv' + \mu - h)(iv' + \mu - h - U)} \\ &+ \frac{n_{\uparrow} - 1}{(iv' + i\omega + \mu - h)(iv' + \mu - h)(iv + \mu + h - U)} + \frac{1 - n_{\uparrow}}{(iv + i\omega + \mu + h - U)(iv + \mu + h - U)(iv' + \mu - h)} \\ &+ \frac{1 - n_{\downarrow}}{(iv + i\omega + \mu + h)(iv' + \mu - h - U)(iv + \mu + h - U)} + \frac{n_{\downarrow} - 1}{(iv + i\omega + \mu + h)(iv + \mu + h - U)(iv' + i\omega + \mu - h)} \\ &+ \frac{1 - n_{\downarrow}}{(iv' + \mu - h)(iv + i\omega + \mu + h)(iv' + i\omega + \mu - h)} + \frac{1 - n_{\downarrow}}{(iv' + \mu - h)(iv + i\omega + \mu + h)(iv + \mu + h)} \\ &+ \frac{1 - n_{\downarrow}}{(iv' + \mu - h - U)(iv + \mu + h)(iv' + i\omega + \mu - h - U)} + \frac{n_{\downarrow} - 1}{(iv' + \mu - h - U)(iv + i\omega + \mu + h)(iv + \mu + h)} \\ &+ \frac{1 - n_{\downarrow}}{(iv + i\omega + \mu + h - U)(iv + \mu + h)(iv' + i\omega + \mu - h - U)} + \frac{n_{\downarrow} - 1}{(iv' + \mu - h)(iv + i\omega + \mu + h - U)(iv + \mu + h)} \\ &+ \frac{-n_{\uparrow}}{(iv' + \mu - h - U)(iv + i\omega + \mu + h - U)(iv' + i\omega + \mu - h - U)} \\ &+ \frac{-n_{\uparrow}}{(iv' + \mu - h - U)(iv + i\omega + \mu + h - U)(iv + \mu + h - U)}, \end{aligned} \quad (\text{D3})$$

where

$$n_{\sigma} = \frac{e^{(\mu+\sigma h)\beta} + e^{(2\mu-U)\beta}}{1 + e^{(\mu+h)\beta} + e^{(\mu-h)\beta} + e^{(2\mu-U)\beta}} \quad (\text{D4})$$

and $G_{2,\downarrow\downarrow}^{\text{con}}$ and $G_{2,\uparrow\downarrow}^{\text{con}}$ can be obtained from Eqs. (D2) and (D3) by changing h to $-h$. Note that the terms in the first two lines in Eq. (D3) can become singular (i.e., proportional to $\delta_{v,v'+\omega}$ and $\delta_{v,v'}$) for $\mu = U/2$ and $h = 0$, respectively; in these cases, the limit has to be taken carefully.

With these building blocks we can calculate all generalized susceptibilities of the HA: The $\sigma\sigma'$ spin indices can be calculated directly with Eqs. (D5) and (D6),

$$\chi_{\sigma\sigma}^{v,v',\omega} = G_{2,\sigma\sigma}^{\text{con}}(v, v', \omega) + \chi_{0,\sigma\sigma}^{v,v',\omega}, \quad (\text{D5})$$

$$\chi_{\sigma\sigma'}^{v,v',\omega} = G_{2,\sigma\sigma'}^{\text{con}}(v, v', \omega) \quad \text{with } \sigma \neq \sigma'. \quad (\text{D6})$$

The spin indices $\overline{\sigma\sigma'}$ can be calculated with

$$\chi_{\overline{\sigma\sigma'}}^{v,v',\omega} = -\chi_{\sigma\sigma'}^{v,v+\omega,v-v'} + \chi_{0,\overline{\sigma\sigma'}}^{v,v',\omega}, \quad (\text{D7})$$

where $\sigma \neq \sigma'$ [38] and the bubble terms χ_0 are defined in Eqs. (G1) and (G2).

Finally, the generalized susceptibilities in the particle-particle channel can be calculated by performing the frequency shift $\omega \rightarrow \omega - v - v'$.

APPENDIX E: PROJECTED WEIGHT IN THE COUPLED LONGITUDINAL CHANNEL

To quantify how much an eigenvalue of χ_L is attributed to either the charge or the spin subspace, respectively, we split each eigenvector v [normalized by $\| \cdot \|_T$ in Eq. (A15)] into the

charge and spin subspaces

$$v = \begin{pmatrix} v_c \\ v_s \end{pmatrix}. \quad (\text{E1})$$

In doing so, we can assign each eigenvector a projected weight which gives the percentage contribution of the eigenvector in the charge/spin subspace $\mathcal{N}_c/\mathcal{N}_s$ with

$$\mathcal{N}_{c/s} = \frac{\|v_{c/s}\|_{\dagger}^2}{\|v\|_{\dagger}^2}, \quad (\text{E2})$$

where $\mathcal{N}_c + \mathcal{N}_s = 1$ and $\|u\|_{\dagger}^2 = u^{\dagger} \cdot u$ [78].

To prove that pseudodivergences with $SU(2)_P$ symmetry ($\delta\mu = 0$) are always maximally ‘‘mixed’’ ($\mathcal{N}_c = \mathcal{N}_s = 0.5$), we first note that the Shiba mapping connects the $SU(2)_P$ symmetric case with the $SU(2)_S$ symmetric case ($h = 0$), where the charge and the spin channel are decoupled centro-Hermitian matrices.

We consider the eigenvectors v_1 and v_2 of a complex-conjugate pair of eigenvalues of the generalized susceptibility in the charge or the spin channel. Because of Eq. (A16), the symmetric and antisymmetric parts of v_1 can be written as

$$v_1 = \frac{1}{2}(v_1 + v_2^*) + \frac{1}{2}(v_1 - v_2^*) \text{ with } v_{S/A} = \frac{1}{2}(v_1 \pm v_2^*). \quad (\text{E3})$$

As we know from Eq. (C18), only the symmetric part of the eigenvector gets mapped from the charge/spin subspace to the spin/charge subspace.

Therefore, we must calculate the norm only for the symmetric/antisymmetric part of the eigenvector,

$$\begin{aligned} \frac{\|v_{S/A}\|_{\dagger}^2}{\|v_1\|_{\dagger}^2} &= \frac{1}{4\|v_1\|_{\dagger}^2} (v_1^{\dagger} \cdot v_1 \pm v_2^T \cdot v_1 \pm v_1^{\dagger} \cdot v_2^* + v_2^T \cdot v_2^*) \\ &= \frac{1}{2}, \end{aligned} \quad (\text{E4})$$

where $v_1^T \cdot v_2 = 0$ and $\|v_2\|_{\dagger} = \|v_1\|_{\dagger}$ [79].

Hence, we find that complex-conjugate pairs, and therefore pseudodivergences, have the maximal mixing ($\mathcal{N}_c = \mathcal{N}_s = 0.5$) between the charge and longitudinal spin subspace when $SU(2)_P$ symmetry is fulfilled.

APPENDIX F: $T = 0$ LIMIT OF THE HUBBARD ATOM

The advantage of considering a *dimensionless* parameter space of $\{\beta\delta\mu, \beta h, \beta U\}$ in the main text allows also for an intuitive understanding of the $T \rightarrow 0$ limit.

In Fig. 8, the first loop and the first parabola divergence line structure in the charge channel for the $SU(2)_S$ symmetric case are shown for different inverse temperatures $\beta = 1/T$.

Here, we observe that, for $T \rightarrow 0$ ($\beta \rightarrow \infty$), the loop structure contracts to a single point, and both exceptional points of the parabola approach $\delta\mu = 0$.

The scaling suggested by the $T \rightarrow 0$ evolution of divergence lines shown in Fig. 8 outlines an intuitive procedure to get a first understanding of the $T = 0$ vertex divergence properties. This procedure generally works satisfactorily, except for the discontinuous parts of the phase space, located at $\delta\mu = 0$ for $U < 0$ and at $\delta\mu = \pm U/2$ for $U > 0$. In particular, since the generalized susceptibility matrix becomes Hermitian for $\delta\mu = 0$, the exceptional points must transform either continuously into two degenerate or discontinuously

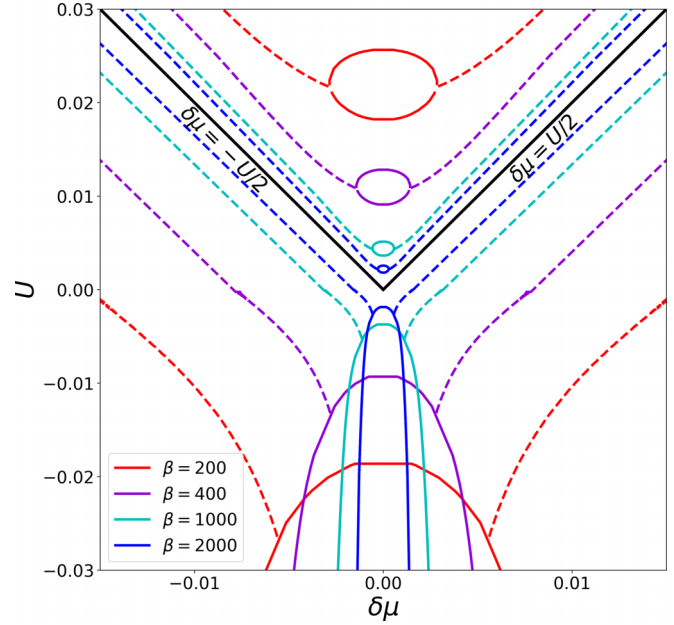


FIG. 8. The phase space diagram of the first loop and parabola divergence line structure in the charge channel for different temperatures for the $SU(2)_S$ symmetric case ($h = 0$).

into two separate eigenvalues of two linear-independent eigenvectors (one symmetric, one antisymmetric). By carefully evaluating the analytical expressions at $\delta\mu = 0$ and $T = 0$ (see Refs. [22,70]), we find a single vanishing eigenvalue with an antisymmetric eigenvector for every $U < 0$ and $\delta\mu = 0$ at $T = 0$, where the model is discontinuous. On the other hand, for $U > 0$ where no discontinuity appears, one finds two degenerate vanishing eigenvalues (one with a symmetric eigenvector and one with an antisymmetric eigenvector) for every $U > 0$ and $\delta\mu = 0$ at $T = 0$. This behavior matches the $T \rightarrow 0$ evolution that the loop structures formed by a symmetric and an antisymmetric divergence that contracts to a single point.

Further, we find that the pseudodivergence lines (at $\delta\mu \neq 0$) become parallel to $\delta\mu = \pm U/2$ in the limit of $U, \delta\mu \rightarrow \infty$, which mark the boundaries of a V-shaped region in the phase diagram. Thus, the pseudodivergences that stem from the loop structure at $U > 0$ remain inside this V-shaped region ($U > 2|\delta\mu|$), and the pseudodivergences that emerge from the parabolas at $U < 0$ stay outside of it ($U < 2|\delta\mu|$).

Applying the same analysis to the spin and pairing channel, one can show that the pairing divergences are confined inside the V-shaped area while the spin pseudodivergences stay outside of it. From these intuitive considerations, we can schematically draw Fig. 3 in the main text.

In principle, a more rigorous treatment of the $T = 0$ limit, which yield, however, the same results [80], can be performed as explained in Ref. [70]. In particular, for the analytical expressions of the generalized susceptibility reported in Appendix D, one has to take into account that the Matsubara frequencies become continuous and can no longer be regarded as matrix indices.

Consequently for $T = 0$, a sum over Matsubara frequencies becomes an integral, and a Kronecker δ in Matsubara

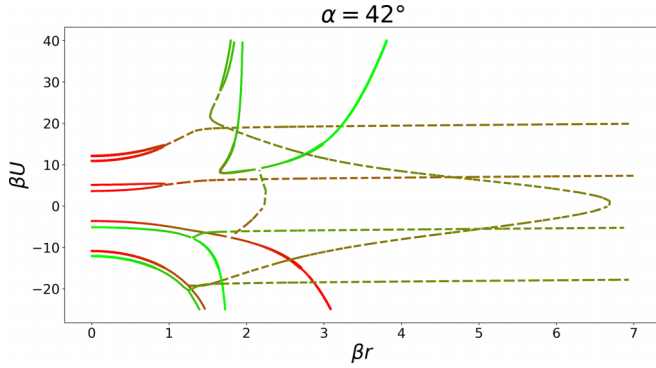


FIG. 9. The phase space diagrams of the vertex (pseudo)divergences in the coupled longitudinal channel for the Hubbard atom are shown. Note that the first two divergence line structures are displayed. The plotting conventions are as in Fig. 2.

frequencies becomes a Dirac δ :

$$\frac{1}{\beta} \sum_v \xrightarrow{\beta \rightarrow \infty} \int_{-\infty}^{\infty} \frac{dv}{2\pi}, \quad (\text{F1})$$

$$\beta \delta_{vv'} \xrightarrow{\beta \rightarrow \infty} 2\pi \delta(v - v'), \quad (\text{F2})$$

$$\beta \delta_{\omega 0} \xrightarrow{\beta \rightarrow \infty} 2\pi \delta(\omega). \quad (\text{F3})$$

For the remaining terms in the analytical formulas in Appendix D, we take the limit $\beta \rightarrow \infty$.

APPENDIX G: ADDITIONAL INFORMATION ON VERTEX DIVERGENCE STRUCTURE

In this Appendix, we will give some additional information about the vertex (pseudo)divergence phase diagram.

To get started, we show the first two vertex (pseudo)divergence line structures in the coupled longitudinal channel for $\alpha = 42^\circ$ in Fig. 9.

In addition to the first divergence line loop, we find a second loop at higher U values for $U > 0$. On the other hand, for $U < 0$ we find a second pair of parabolas. Furthermore, we find a second parabola for $U > 0$ at smaller r values than the first parabola at $U > 0$. The pseudodivergence that is adjoined to the second parabola takes a large detour to high r values and then goes back to the parabola pair at negative $U < 0$.

To investigate the pseudodivergences at $U = 0$, we just have to consider the bubble term χ_0 of the susceptibility. The

bubble term in the spin index space is defined as

$$\chi_{0,\sigma\sigma'}^{v,v',\omega} = -\beta G_\sigma(v) G_{\sigma'}(v + \omega) \delta_{vv'} \delta_{\sigma\sigma'}, \quad (\text{G1})$$

$$\chi_{0,\sigma\sigma'}^{v,v',\omega} = -\beta G_\sigma(v) G_{\sigma'}(v + \omega) \delta_{vv'}, \quad (\text{G2})$$

$$\chi_{0,\sigma\sigma',pp}^{v,v',\omega} = -\beta G_\sigma(v) G_{\sigma'}(\omega - v) \delta_{vv'} \quad (\text{G3})$$

for the longitudinal and transversal spin channel in ph and pp frequency convention. χ_0 in the longitudinal channel reads

$$\chi_{0,L} = \begin{pmatrix} \chi_{0,\uparrow\uparrow} + \chi_{0,\downarrow\downarrow} & \chi_{0,\uparrow\uparrow} - \chi_{0,\downarrow\downarrow} \\ \chi_{0,\uparrow\uparrow} - \chi_{0,\downarrow\downarrow} & \chi_{0,\uparrow\uparrow} + \chi_{0,\downarrow\downarrow} \end{pmatrix}. \quad (\text{G4})$$

Note that $\chi_{0,L}$ is only diagonal for $SU(2)_S$ symmetric systems, but it can be diagonalized by

$$P \chi_{0,L} P = \begin{pmatrix} \chi_{0,\uparrow\uparrow} & 0 \\ 0 & \chi_{0,\downarrow\downarrow} \end{pmatrix} \quad \text{with} \quad P = \begin{pmatrix} \mathbb{1} & \mathbb{1} \\ \mathbb{1} & -\mathbb{1} \end{pmatrix}, \quad (\text{G5})$$

where P transforms from the spin index basis to the longitudinal (physical) channel. Further, the bubble terms for the transversal spin and the pairing channel are defined as

$$\chi_{0,S_x} = \chi_{0,\uparrow\downarrow} + \chi_{0,\downarrow\uparrow}, \quad (\text{G6})$$

$$\chi_{0,\text{pair}} = -\chi_{0,\uparrow\downarrow,pp} - (\chi_{0,\downarrow\uparrow,pp})^*. \quad (\text{G7})$$

By replacing G_σ with $G_{0,\sigma}$ and by solving for $\text{Re}(\chi_0) = 0$, we find the pseudodivergences for $U = 0$ and $\omega = 0$. The resulting conditions for the different channels are the following:

$$\chi_{0,\uparrow\uparrow}: \quad r = \frac{v}{\sqrt{1 + 2 \cos \alpha \sin \alpha}}, \quad (\text{G8})$$

$$\chi_{0,\downarrow\downarrow}: \quad r = \frac{v}{\sqrt{1 - 2 \cos \alpha \sin \alpha}}, \quad (\text{G9})$$

$$\chi_{0,S_x}: \quad r = \frac{v}{\sqrt{(\cos \alpha)^2 - (\sin \alpha)^2}}, \quad (\text{G10})$$

$$\chi_{0,\text{pair}}: \quad r = \frac{v}{\sqrt{(\sin \alpha)^2 - (\cos \alpha)^2}}. \quad (\text{G11})$$

Therefore, for $\chi_{0,\uparrow\uparrow}$ and $\chi_{0,\downarrow\downarrow}$, two pseudodivergences cross the $U = 0$ axis for almost all values of α except for $\alpha = 45^\circ$, where only the pseudodivergences of $\chi_{0,\downarrow\downarrow}$ are present at $U = 0$. By transforming the eigenvectors back in the space of the longitudinal channel, we find that all pseudodivergences at $U = 0$ are maximally ‘‘mixed’’ ($\mathcal{N}_c = \mathcal{N}_s = 0.5$).

In the transversal spin channels, pseudodivergences cross the $U = 0$ axis only for $0^\circ \leq \alpha < 45^\circ$ and for the pairing channel only for $45^\circ < \alpha \leq 90^\circ$.

- [1] M. Liu, L. W. Harriger, H. Luo, M. Wang, R. A. Ewings, T. Guidi, H. Park, K. Haule, G. Kotliar, S. M. Hayden, and P. Dai, Nature of magnetic excitations in superconducting $\text{BaFe}_{1.9}\text{Ni}_{0.1}\text{As}_2$, *Nat. Phys.* **8**, 376 (2012).
- [2] A. Hausoel, M. Karolak, E. Şaşıoğlu, A. Lichtenstein, K. Held, A. Katanin, A. Toschi, and G. Sangiovanni, Local magnetic moments in iron and nickel at ambient and Earth’s core conditions, *Nat. Commun.* **8**, 16062 (2017).
- [3] D. Vilardi, C. Taranto, and W. Metzner, Dynamically enhanced magnetic incommensurability: Effects of local dynamics on

nonlocal spin correlations in a strongly correlated metal, *Phys. Rev. B* **97**, 235110 (2018).

- [4] C. Watzenböck, M. Edelmann, D. Springer, G. Sangiovanni, and A. Toschi, Characteristic timescales of the local moment dynamics in Hund’s metals, *Phys. Rev. Lett.* **125**, 086402 (2020).
- [5] C. Watzenböck, M. Fellingner, K. Held, and A. Toschi, Long-term memory magnetic correlations in the Hubbard model: A dynamical mean-field theory analysis, *SciPost Phys.* **12**, 184 (2022).

- [6] A. Kauch, P. Pudleiner, K. Astleithner, P. Thunström, T. Ribic, and K. Held, Generic optical excitations of correlated systems: π -tons, *Phys. Rev. Lett.* **124**, 047401 (2020).
- [7] A. Vranić, J. Vučićević, J. Kokalj, J. Skolimowski, R. Žitko, J. Mravlje, and D. Tanasković, Charge transport in the Hubbard model at high temperatures: Triangular versus square lattice, *Phys. Rev. B* **102**, 115142 (2020).
- [8] J. Vučićević, S. Predin, and M. Ferrero, Charge fluctuations, hydrodynamics, and transport in the square-lattice Hubbard model, *Phys. Rev. B* **107**, 155140 (2023).
- [9] O. Gunnarsson, T. Schäfer, J. P. F. LeBlanc, E. Gull, J. Merino, G. Sangiovanni, G. Rohringer, and A. Toschi, Fluctuation diagnostics of the electron self-energy: Origin of the pseudogap physics, *Phys. Rev. Lett.* **114**, 236402 (2015).
- [10] W. Wu, M. Ferrero, A. Georges, and E. Kozik, Controlling Feynman diagrammatic expansions: Physical nature of the pseudogap in the two-dimensional Hubbard model, *Phys. Rev. B* **96**, 041105(R) (2017).
- [11] G. Rohringer, Spectra of correlated many-electron systems: From a one- to a two-particle description, *J. Electron Spectrosc. Relat. Phenom.* **241**, 146804 (2020).
- [12] T. Schäfer and A. Toschi, How to read between the lines of electronic spectra: The diagnostics of fluctuations in strongly correlated electron systems, *J. Phys.: Condens. Matter* **33**, 214001 (2021).
- [13] W. Wú, X. Wang, and A.-M. Tremblay, Non-Fermi liquid phase and linear-in-temperature scattering rate in overdoped two-dimensional Hubbard model, *Proc. Natl. Acad. Sci. USA* **119**, e2115819119 (2022).
- [14] X. Dong, L. Del Re, A. Toschi, and E. Gull, Mechanism of superconductivity in the Hubbard model at intermediate interaction strength, *Proc. Natl. Acad. Sci. USA* **119**, e2205048119 (2022).
- [15] G. Rohringer, H. Hafermann, A. Toschi, A. A. Katanin, A. E. Antipov, M. I. Katsnelson, A. I. Lichtenstein, A. N. Rubtsov, and K. Held, Diagrammatic routes to nonlocal correlations beyond dynamical mean field theory, *Rev. Mod. Phys.* **90**, 025003 (2018).
- [16] F. Krien, A. Valli, and M. Capone, Single-boson exchange decomposition of the vertex function, *Phys. Rev. B* **100**, 155149 (2019).
- [17] F. Krien, A. Valli, P. Chalupa, M. Capone, A. I. Lichtenstein, and A. Toschi, Boson-exchange parquet solver for dual fermions, *Phys. Rev. B* **102**, 195131 (2020).
- [18] L. Del Re, M. Capone, and A. Toschi, Dynamical vertex approximation for the attractive Hubbard model, *Phys. Rev. B* **99**, 045137 (2019).
- [19] L. Del Re and A. Toschi, Dynamical vertex approximation for many-electron systems with spontaneously broken SU(2) symmetry, *Phys. Rev. B* **104**, 085120 (2021).
- [20] G. Rohringer, A. Valli, and A. Toschi, Local electronic correlation at the two-particle level, *Phys. Rev. B* **86**, 125114 (2012).
- [21] H. Hafermann, Self-energy and vertex functions from hybridization-expansion continuous-time quantum Monte Carlo for impurity models with retarded interaction, *Phys. Rev. B* **89**, 235128 (2014).
- [22] P. Thunström, O. Gunnarsson, S. Ciuchi, and G. Rohringer, Analytical investigation of singularities in two-particle irreducible vertex functions of the Hubbard atom, *Phys. Rev. B* **98**, 235107 (2018).
- [23] F. B. Kugler, S.-S. B. Lee, and J. von Delft, Multipoint correlation functions: Spectral representation and numerical evaluation, *Phys. Rev. X* **11**, 041006 (2021).
- [24] A. Ge, J. Halbinger, S.-S. B. Lee, J. von Delft, and F. B. Kugler, Analytic continuation of multipoint correlation functions, *Ann. Phys.* **2300504** (2024).
- [25] J. Kuneš, Efficient treatment of two-particle vertices in dynamical mean-field theory, *Phys. Rev. B* **83**, 085102 (2011).
- [26] A. Tagliavini, S. Hummel, N. Wentzell, S. Andergassen, A. Toschi, and G. Rohringer, Efficient Bethe-Salpeter equation treatment in dynamical mean-field theory, *Phys. Rev. B* **97**, 235140 (2018).
- [27] N. Wentzell, G. Li, A. Tagliavini, C. Taranto, G. Rohringer, K. Held, A. Toschi, and S. Andergassen, High-frequency asymptotics of the vertex function: Diagrammatic parametrization and algorithmic implementation, *Phys. Rev. B* **102**, 085106 (2020).
- [28] S.-S. B. Lee, F. B. Kugler, and J. Von Delft, Computing local multipoint correlators using the numerical renormalization group, *Phys. Rev. X* **11**, 041007 (2021).
- [29] D. Springer, P. Chalupa, S. Ciuchi, G. Sangiovanni, and A. Toschi, Interplay between local response and vertex divergences in many-fermion systems with on-site attraction, *Phys. Rev. B* **101**, 155148 (2020).
- [30] T. Schäfer, G. Rohringer, O. Gunnarsson, S. Ciuchi, G. Sangiovanni, and A. Toschi, Divergent precursors of the Mott-Hubbard transition at the two-particle level, *Phys. Rev. Lett.* **110**, 246405 (2013).
- [31] E. Kozik, M. Ferrero, and A. Georges, Nonexistence of the Luttinger-ward functional and misleading convergence of skeleton diagrammatic series for Hubbard-like models, *Phys. Rev. Lett.* **114**, 156402 (2015).
- [32] O. Gunnarsson, G. Rohringer, T. Schäfer, G. Sangiovanni, and A. Toschi, Breakdown of traditional many-body theories for correlated electrons, *Phys. Rev. Lett.* **119**, 056402 (2017).
- [33] J. Vučićević, N. Wentzell, M. Ferrero, and O. Parcollet, Practical consequences of the Luttinger-ward functional multivaluedness for cluster DMFT methods, *Phys. Rev. B* **97**, 125141 (2018).
- [34] O. Gunnarsson, T. Schäfer, J. P. F. LeBlanc, J. Merino, G. Sangiovanni, G. Rohringer, and A. Toschi, Parquet decomposition calculations of the electronic self-energy, *Phys. Rev. B* **93**, 245102 (2016).
- [35] M. Reitner, P. Chalupa, L. Del Re, D. Springer, S. Ciuchi, G. Sangiovanni, and A. Toschi, Attractive effect of a strong electronic repulsion: The physics of vertex divergences, *Phys. Rev. Lett.* **125**, 196403 (2020).
- [36] P. Chalupa, T. Schäfer, M. Reitner, D. Springer, S. Andergassen, and A. Toschi, Fingerprints of the local moment formation and its kondo screening in the generalized susceptibilities of many-electron problems, *Phys. Rev. Lett.* **126**, 056403 (2021).
- [37] S. Adler, F. Krien, P. Chalupa-Gantner, G. Sangiovanni, and A. Toschi, Non-perturbative intertwining between spin and charge correlations: A “smoking gun” single-boson-exchange result, *SciPost Phys.* **16**, 054 (2024).
- [38] G. Rohringer, New routes towards a theoretical treatment of nonlocal electronic correlations, Ph.D. thesis, TU Wien, 2013.
- [39] M. Reitner, L. Crippa, D. R. Fus, J. C. Budich, A. Toschi, and G. Sangiovanni, Protection of correlation-induced phase instabilities by exceptional susceptibilities, *Phys. Rev. Res.* **6**, L022031 (2024).

- [40] A. Lee, Centrohermitian and skew-centrohermitian matrices, *Lin. Alg. Appl.* **29**, 205 (1980).
- [41] R. D. Hill and S. R. Waters, On κ -real and κ -Hermitian matrices, *Lin. Alg. Appl.* **169**, 17 (1992).
- [42] B. D. Craven, Complex symmetric matrices, *J. Aust. Math. Soc.* **10**, 341 (1969).
- [43] H. Shiba, Thermodynamic properties of the one-dimensional half-filled-band Hubbard model. II: Application of the grand canonical method, *Prog. Theor. Phys.* **48**, 2171 (1972).
- [44] S. Pairault, D. Sénéchal, and A.-M. Tremblay, Strong-coupling perturbation theory of the Hubbard model, *Eur. Phys. J. B* **16**, 85 (2000).
- [45] Note that, for the scope of this paper, we adopt the standard definition of particle-hole transformation, i.e., $c_\sigma \rightarrow c_\sigma^\dagger$. Of course, in principle, one could also choose the alternative definition of $c_\sigma \rightarrow c_{-\sigma}^\dagger$. The latter definition would be consistent with the fact that the particle-hole transformation changes the charge of the particle and therefore also its gyromagnetic moment. This would then be accounted for by flipping the spin in the transformation. Using this alternative definition, the $SU(2)_P$ symmetry would become equivalent to the particle-hole symmetry, and the $SO(4)$ symmetry would be achieved in the presence of simultaneous particle-hole and $SU(2)_S$ symmetry.
- [46] Note that all derivations in this section also hold for non-local generalized susceptibilities of bipartite lattice models if the following criterion is fulfilled: the algebraic sum of the lattice indices of the considered generalized susceptibility is even.
- [47] We recall that the hopping t_{ij} transforms under the Shiba transformation for lattice models as $t_{ij} \rightarrow t_{ij}$ if one index belongs to an odd site and the other an even site, and $t_{ij} \rightarrow \sigma t_{ij}$ otherwise. Hence, if the hopping connects odd to odd or even to even sides (e.g., via a next-nearest-neighborhopping t'), this hopping term would change under the Shiba mapping from t' to $-t'$ for the down electrons only, limiting the potential usefulness of the mapped expressions.
- [48] On an even more general perspective, it is worth mentioning that Eqs. (33) and (36) would hold for the on-site generalized susceptibilities of arbitrary lattice models, albeit with the important caveat that the specific meaning of subindices U and $-U$ needs to be properly reinterpreted. In practice, this can be done by determining the precise effect of the Shiba transformation on the Hamiltonian of the considered model and then defining the meaning of the labels U and $-U$ according to this result.
- [49] A. Georges, G. Kotliar, W. Krauth, and M. J. Rozenberg, Dynamical mean-field theory of strongly correlated fermion systems and the limit of infinite dimensions, *Rev. Mod. Phys.* **68**, 13 (1996).
- [50] T. Schäfer, S. Ciuchi, M. Wallerberger, P. Thunström, O. Gunnarsson, G. Sangiovanni, G. Rohringer, and A. Toschi, Nonperturbative landscape of the Mott-Hubbard transition: Multiple divergence lines around the critical endpoint, *Phys. Rev. B* **94**, 235108 (2016).
- [51] A. A. Abrikosov, L. P. Gorkov, and I. E. Dzyaloshinski, in *Methods of Quantum Field Theory in Statistical Physics*, revised english ed., edited by R. A. Silverman, Dover Books on Physics and Chemistry (Dover, New York, 1975), Chaps. 2 and 3.
- [52] N. E. Bickers, Self-consistent many-body theory for condensed matter systems, in *Theoretical Methods for Strongly Correlated Electrons*, edited by D. Sénéchal, A.-M. Tremblay, and C. Bourbonnais (Springer-Verlag, New York, 2004), pp. 237–296.
- [53] None of the different “bubble” terms $\chi_{r,0}^{v,v',\omega}$ can trigger a divergence, as they are just diagonal in frequency spaces and defined by the product of two Green’s functions.
- [54] E. G. C. P. van Loon, F. Krien, and A. A. Katanin, Bethe-Salpeter equation at the critical end point of the Mott transition, *Phys. Rev. Lett.* **125**, 136402 (2020).
- [55] R. Nourafkan, M. Côté, and A.-M. S. Tremblay, Charge fluctuations in lightly hole-doped cuprates: Effect of vertex corrections, *Phys. Rev. B* **99**, 035161 (2019).
- [56] A. Kowalski, M. Reitner, L. Del Re, M. Chatzieftheriou, A. Amaricci, A. Toschi, L. de’Medici, G. Sangiovanni, and T. Schäfer, Thermodynamic stability at the two-particle level, [arXiv:2309.11108](https://arxiv.org/abs/2309.11108).
- [57] E. G. C. P. van Loon, Second-order phase transitions and divergent linear response in dynamical mean-field theory, *Phys. Rev. B* **109**, L241110 (2024).
- [58] G. Kotliar, S. Y. Savrasov, G. Pálsson, and G. Biroli, Cellular dynamical mean field approach to strongly correlated systems, *Phys. Rev. Lett.* **87**, 186401 (2001).
- [59] T. A. Maier, M. Jarrell, T. Pruschke, and M. H. Hettler, Quantum cluster theories, *Rev. Mod. Phys.* **77**, 1027 (2005).
- [60] S. Rohshap, Analytical calculation of two-particle vertices for multiorbital Hubbard atom, Master’s thesis, TU Wien, 2023.
- [61] S. Rohshap, M. Wallerberger, and A. Kauch, Analytic results for the two-particle vertex in the atomic limit of the doped Hubbard model (unpublished).
- [62] R. Rossi, F. Werner, N. Prokof’ev, and B. Svistunov, Shifted-action expansion and applicability of dressed diagrammatic schemes, *Phys. Rev. B* **93**, 161102(R) (2016).
- [63] K. V. Houcke, E. Kozik, R. Rossi, Y. Deng, and F. Werner, Physical and unphysical regimes of self-consistent many-body perturbation theory, *SciPost Phys.* **16**, 133 (2024).
- [64] A. J. Kim and E. Kozik, Misleading convergence of the skeleton diagrammatic technique: When the correct solution can be found, [arXiv:2212.14768](https://arxiv.org/abs/2212.14768).
- [65] Note, however, that the presented arguments also apply for non-local susceptibilities with the only difference that the σ index must be interpreted as a combined σ, k index.
- [66] A. Toschi, A. A. Katanin, and K. Held, Dynamical vertex approximation: A step beyond dynamical mean-field theory, *Phys. Rev. B* **75**, 045118 (2007).
- [67] While at this stage we might regard such a coincidence as purely accidental, we note that an almost identical doping level of about 6% for the occurrence of the first EP has also been recently found in numerical calculations for the Anderson impurity model in the wide-band limit [81].
- [68] M. Pelz, S. Adler, M. Reitner, and A. Toschi, Highly non-perturbative nature of the Mott metal-insulator transition: Two-particle vertex divergences in the coexistence region, *Phys. Rev. B* **108**, 155101 (2023).
- [69] Note that, also in this case, we only show the first three parabolas for each channel.
- [70] H. Eßl, Breakdown of the self-consistent perturbation theory beyond particle-hole symmetry, Master’s thesis, TU Wien, 2023.
- [71] More quantitatively, one could observe the following: Along a parabola towards the exceptional point, the percentage of the

- longitudinal spin subspace in the divergences increases. Remarkably, the maximal mixing happens at the exceptional point. Far away from the exceptional point at high βU , the divergences are almost completely in the longitudinal spin subspace. Note that the pseudodivergences in the longitudinal are always maximally mixed (i.e., having weight 0.5 in the charge and the spin subspace) if $SU(2)_S$ symmetry is present, which is shown in Eq. (E4).
- [72] In the coupled longitudinal sector for arbitrary $\delta\mu$ and h , the labeling of a vertex divergence line with N indicates that the corresponding eigenvector has a maximum on the N th Matsubara frequency in the charge or the spin subspace. Since in Fig. 4 only the first divergence line structure is displayed, we show in Fig. 9 also the second divergence line structure for an exemplary case.
- [73] G. Kotliar, S. Murthy, and M. J. Rozenberg, Compressibility divergence and the finite temperature Mott transition, *Phys. Rev. Lett.* **89**, 046401 (2002).
- [74] M. Eckstein, M. Kollar, M. Potthoff, and D. Vollhardt, Phase separation in the particle-hole asymmetric Hubbard model, *Phys. Rev. B* **75**, 125103 (2007).
- [75] A. Stan, P. Romaniello, S. Rigamonti, L. Reining, and J. A. Berger, Unphysical and physical solutions in many-body theories: From weak to strong correlation, *New J. Phys.* **17**, 093045 (2015).
- [76] H. Eßl, M. Reitner, G. Sangiovanni, and A. Toschi, Data and scripts for “General Shiba mapping for on-site four-point correlation functions”, doi:10.48436/k71gw-wm529 (2024).
- [77] The $SO(4)$ symmetric case of Ref. [29] can be obtained by noticing that for $SU(2)_P$ symmetry the matrices have no imaginary part, and for $SU(2)_S$ symmetry χ_{cs} and χ_{sc} vanish.
- [78] Note that for $\mathcal{N}_{c/s}$ other definitions would also be possible, e.g., (a) using $\|v\|_T = 1$ and defining $\mathcal{N}_{c/s} = \|v_{c/s}\|_T$. However, since $\mathcal{N}_{c/s} \in \mathbb{C}$, this definition cannot be used to define a percentage. (b) Using $\|v\|_{\dagger} = 1$ and defining $\mathcal{N}_{c/s} = \|v_{c/s}\|_{\dagger}$. This definition is in fact equivalent to the definition in Eq. (E2). However, vectors normalized with $\|\cdot\|_T$ have the convenient property of either symmetric or antisymmetric real and imaginary parts in the charge and spin subspaces (if their eigenvalue is real). Hence, it is more practical to work with these vectors. The equivalence can be shown by comparing the two different normalizations of the same vector v : $\tilde{v} = \frac{v'}{\|v'\|_{\dagger}} e^{i\varphi}$, where $\|\tilde{v}\|_{\dagger} = 1$, $\|v'\|_T = 1$, and φ is the phase of $\|\tilde{v}\|_T$. The additional factor $1/\|v\|_{\dagger}^2$ in the definition of the projected weight assures $\mathcal{N}_c + \mathcal{N}_s = 1$.
- [79] $v_1^T \cdot v_2 = 0$, because the vectors are orthogonal regarding the scalar product Eq. (A14). Further, $\|v_2\|_{\dagger} = \|v_1\|_{\dagger}$ holds because of the relation $v_2 = Jv_1^*$.
- [80] Indeed, the results obtained with the simple scaling argument of the dimensionless phase space agree well with the results from the more rigorous treatment of the $T \rightarrow 0$ limit of the analytical formulas, where only special care has to be taken for the discontinuous parts of the phase space. This shows the usefulness of the dimensionless phase space.
- [81] L. Domazetovsky, Divergences of the irreducible vertex beyond particle-hole symmetry: An Anderson impurity model study, Project work, TU Wien, 2022.